REVIEW

ADVANCED
ENERGY & SUSTAINABILITY
RESEARCH
Open Access

www.advenergysustres.com

p-Type Redox-Active Organic Electrode Materials for Next-Generation Rechargeable Batteries

Hyojin Kye, Yeongkwon Kang, Deogjin Jang, Ji Eon Kwon,* and Bong-Gi Kim*

p-Type redox-active organic materials (ROMs) draw increasing attention as a promising alternative to conventional inorganic electrode materials in secondary batteries due to high redox voltage, fast rate capability, environment friendliness, and abundance. First, fundamental properties of the p-type ROMs regarding the energy levels and the anion-related chemistry are briefly introduced. Then, the development progress of the p-type ROMs is outlined in this review by classifying them according to their redox centers. The molecular design strategies employed for improving their electrochemical performance are discussed to guide further research. Finally, a summary of the electrochemical performance achieved, regarding voltage, specific energy with power, and cycle stability, is provided with perspectives.

1. Introduction

Efficient energy storage systems are crucial for realizing sustainable daily life using portable electronic devices, electric vehicles (EVs), and smart grids.[1] The rapid development of lithium-ion batteries (LIBs) relying on inorganic electrode materials such as $LiCoO_2$,[2,3] $LiFePO_4$,[4] and $LiMn_2O_4$[5] has facilitated inexpensive mobile energy storage devices with high energy density so far.[6,7] However, their rigid crystalline structures impede ionic transportation, resulting in sluggish rate capability (**Figure 1**a). Furthermore, it is predicted that the scarcity of Li and Co resources will hinder the mass production of large-scale LIBs to keep up with the steeply increasing various demands.[8] In addition, the use of such toxic metals restricts

H. Kye, Y. Kang, D. Jang, B.-G. Kim
Department of Organic and Nano System Engineering
Konkuk University
Seoul 05029, Korea
E-mail: bgkim2015@konkuk.ac.kr

J. E. Kwon
Functional Composite Materials Research Center
Korea Institute of Science and Technology (KIST)
Jeonbuk 55324, Republic of Korea
E-mail: jekwon@kist.re.kr

The ORCID identification number(s) for the author(s) of this article can be found under https://doi.org/10.1002/aesr.202200030.

the recycling of LIBs and causes environmental pollution. Therefore, as an alternative charge-carrying ion to the lithium, more abundant metals such as sodium[9,10] and potassium,[11–14] which belong to the same group with Li, or multivalent elements such as aluminum,[15] magnesium,[16] and zinc[17–19] have been explored. However, a lack of reliable inorganic electrode materials still disrupts their practical use.

Recently, redox-active organic materials (ROMs), which are composed of elements such as C, O, N, and S, have emerged as a promising alternative to inorganic electrode materials owing to their abundance, light weight, and environmental impact benignity.[20–24] Typically, the redox reactions of ROMs are not limited by choice of counterions, enabling versatile use of them as electrode materials in various types of batteries, including metal-ion,[25–27] dual-ion,[28–31] molecular-ion,[32–34] and anion-shuttle batteries.[35,36] The flexible nature of intermolecular packing can potentially provide higher rate capability of ROMs than the inorganic electrode materials.[20,24] Furthermore, ROMs allow us to tailor their physicochemical and electrochemical properties by elaborate molecular design.[37,38] However, ROMs still suffer from low electrical conductivity and high solubility in the electrolytes (Figure 1a).

According to Hünig's classification, the redox reaction of ROMs is classified into three different types (i.e., p-, n-, and bipolar-type) depending on the intake/release of electrons and counterions.[21,39–41] As shown in Figure 1b, a p-type ROM (**P**) reversibly undergoes oxidation to form a positively charged state (**P**$^+$) by losing an electron, and its charge is compensated by a counter anion (**A**$^-$) (e.g., PF_6^-, TFSI$^-$, etc.) in the electrolyte. In contrast, an n-type ROM (**N**) is reduced to form a negatively charged state (**N**$^-$) by accepting an electron, and a counter cation (**M**$^+$) (e.g., Li$^+$ and other metal ions) participates in the redox reaction to compensate the negative charge. A bipolar-type ROM has both n- and p-type redox features in a single molecule, producing negatively or positively charged states by reversible reduction or oxidation, respectively.

In the 1980s, along with the discovery of conducting polymers (CPs), many attempts have been made to utilize them for an electrode material in secondary batteries (Figure 1c).[42–45] Typically, the CPs, including polythiophene (PTh), polypyrrole (PPy), and polyaniline (PANI), can be oxidized by accepting anions. Such p-type doping process considerably increases the electrical conductivity of the CPs. Despite their high electrical conductivity, slopy voltage profiles and low specific capacities due to limited p-type doping degree hindered further research.
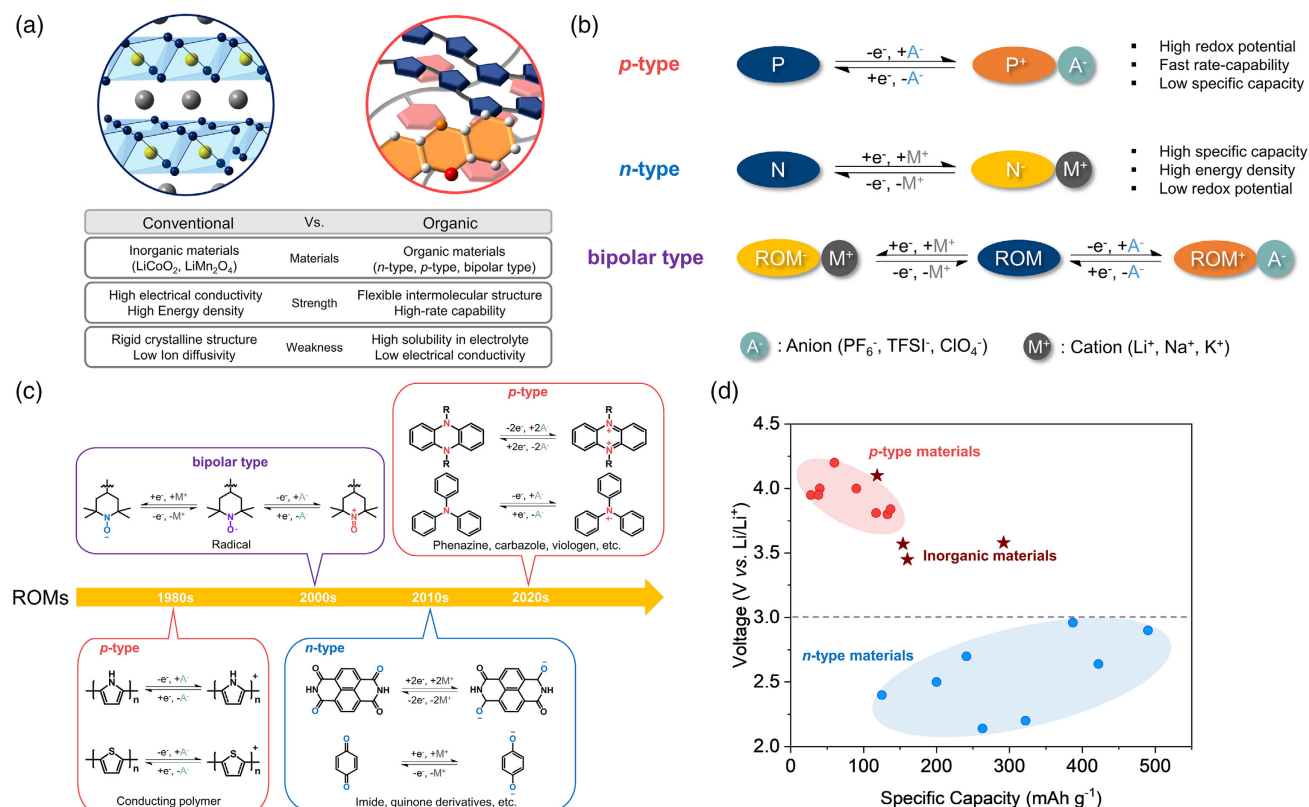
Figure 1. a) Pros and cons of conventional inorganic and organic electrode materials. b) The classification of organic electrode materials depending on their redox mechanism: p-, n-, and bipolar-type redox-active organic materials (ROMs). c) The development timeline of organic electrode materials with the representative ROMs. d) Voltage–capacity plots of reported ROMs and conventional inorganic materials.

In the early 2000s, the nitroxide radical polymers showing bipolar-type redox characteristics with distinct voltage plateaus were proposed as an organic cathode material.[46,47] As shown in Figure 1c, a 2,2,6,6-tetramethyl piperidinyloxyl (TEMPO) radical, the most representative nitroxide, can undergo either a single-electron oxidation (p-type) or a single-electron reduction (n-type) by accepting an anion or cation, respectively. In their initial studies, because of low electrical conductivity and high solubility, they were problematic for practical application; however, great efforts to make breakthroughs have continued,[48–51] which inspired many researchers to get interested in the organic electrode materials.

After that, numerous papers reporting organic electrode materials have been published, so far, but most of the studies have focused on n-type ROMs.[52–59] Generally, many n-type ROMs undergo multi-electron redox reactions to provide high specific capacity. For example, benzoquinone,[60] anthraquinone,[61] terephthalate,[62,63] and imide[64] derivatives were reported to deliver 490, 225, 241, and 200 mAh g^{-1} of specific capacity, respectively, relying on two stepwise single-electron reductions (see examples for the n-type ROMs in Figure 1c). Their specific capacities are much larger than those of inorganic electrode materials (Figure 1d). However, the redox voltages of the n-type ROMs are typically limited below 3.0 V versus Li/Li$^+$, which is much inferior to conventional cathode materials due to their redox mechanism.

Naturally, growing attention is recently paid to the p-type ROMs having high redox voltages (>3.5 V vs Li/Li$^+$), such as phenazine (PNZ),[65–67] carbazole,[68,69] and phenylamine derivatives.[70,71] Such p-type ROMs undergo reversible oxidations to form cationic species (see examples for the p-type ROMs in Figure 1c). In contrast to the n-type ROMs, the redox reactions of the p-type ROMs involve bulky counter anions to compensate for the positive charges, potentially leading to faster rate performance.[41,72] However, despite the promising potential, review papers comprehensively dealing with the p-type ROMs are scarcely reported to date. Therefore, in this article, we mainly focus on the p-type ROMs for electrode materials in secondary batteries, aiming at providing a perspective for properly designing them to improve electrochemical performance. Over the past decade, a lot of p-type ROMs based on various kinds of redox centers have been reported. This review starts with the fundamental characteristics of the p-type ROMs related to the redox voltages and kinetics, including the energy level and counter anion effects. Then, the reported p-type ROMs, so far, are classified depending on their redox centers into CPs, phenylamines, dibenzo-annulated five-membered rings, dibenzo-annulated six-membered rings, nitroxide radicals, viologens, and other miscellaneous centers. In each section covering the respective redox centers, we address their redox mechanism and fundamental electrochemical properties, including redox voltages and theoretical specific capacities. Subsequently, we introduce

molecular design strategies to improve redox voltage, practical specific capacity, energy density, cycle stability, and rate capability. Finally, comparisons of the electrochemical performance are given to provide a bird's eye view of the p-type ROMs with prospects. In this work, we deal with only p-type ROMs for stationary-type batteries. Since this review mainly deals with lithium–organic batteries, aqueous batteries based on multivalent metals are not covered in here. For comprehensive reviews on aqueous batteries, the referred reviews would be helpful.[73–75] To get further information on other types of batteries such as redox-flow batteries, other excellent reviews would be helpful.[76–79]

2. Fundamental Electrochemical Properties

2.1. Redox Potential and Energy Level

Redox potential is the tendency of a chemical species to acquire or lose electrons. Thus, the redox potential of ROMs is determined by their frontier molecular orbital (FMO) energy levels depending on the redox mechanism type (**Figure 2**a). For example, the n-type materials tend to be reduced by accepting electrons via the lowest unoccupied molecular orbital (LUMO, i.e., electron affinity). Accordingly, one can conveniently tune the redox potential of n-type ROMs by adjusting their LUMO level through the substitution of heteroatoms and functional groups. The relationship between the LUMO energy level and the redox potential of n-type ROMs was systematically studied by several research groups.[27,61,80–82] Song et al. investigated a series of polyimides that possessed different sizes of aromatic cores.[82] It was shown that the LUMO level of the polyimides was deepened as the core size was enlarged, leading to the elevation of the redox potential. Similarly, Liang et al. designed

four anthraquinone derivatives with different heteroatomic aromatic rings, including furan, thiophene, pyridine, and benzene.[61] It was clearly revealed that their redox potentials correlated well with the LUMO levels. Based on the results, considerable efforts have been made to elevate the redox potential of n-type ROMs above 3.0 V versus Li/Li^+ (i.e., LUMO < −4.4 eV) where the reduced products (i.e., N^-M^+) can acquire the air stability.[83,84] However, only a few n-type ROMs[83,85–87] possessing such a deep LUMO level were reported to date, which hinders the organic electrode materials from becoming a game changer in the metal-ion battery technology.

In sharp contrast, a high redox voltage over 3.5 V verus Li/Li^+ can be expected in the p-type ROMs because the electrons are eliminated from the deeper highest occupied molecular orbital (HOMO, i.e., ionization potential) when they undergo oxidation (Figure 2a). For instance, phenylamine (Section 3.2)[70] and carbazole (Cbz, Section 3.3)[69] derivatives, bearing a nitrogen redox center, show a single electron oxidation at around 3.6–3.8 V versus Li/Li^+ (Figure 2b). But, due to the single redox, they typically deliver a specific capacity lower than 100 mAh g^{-1}, resulting in a low specific energy. We will introduce several design strategies to elevate their redox potential as well as specific capacity and thus to increase specific energy in those sections.

Meanwhile, N,N'-substituted PNZ compounds (Section 3.4.1), which have two nitrogen redox centers in a fused six-membered aromatic ring, were reported to show double redox at 3.1 and 3.7 V versus Li/Li^+.[65] Despite large specific capacity (>200 mAh g^{-1}) by the aid of double redox, the redox potential of PNZ is lower than conventional inorganic electrode materials. Therefore, to endow with higher redox potential, various PNZ derivatives where the nitrogen atoms were substituted by other heteroatoms (i.e., S and O) were proposed, including
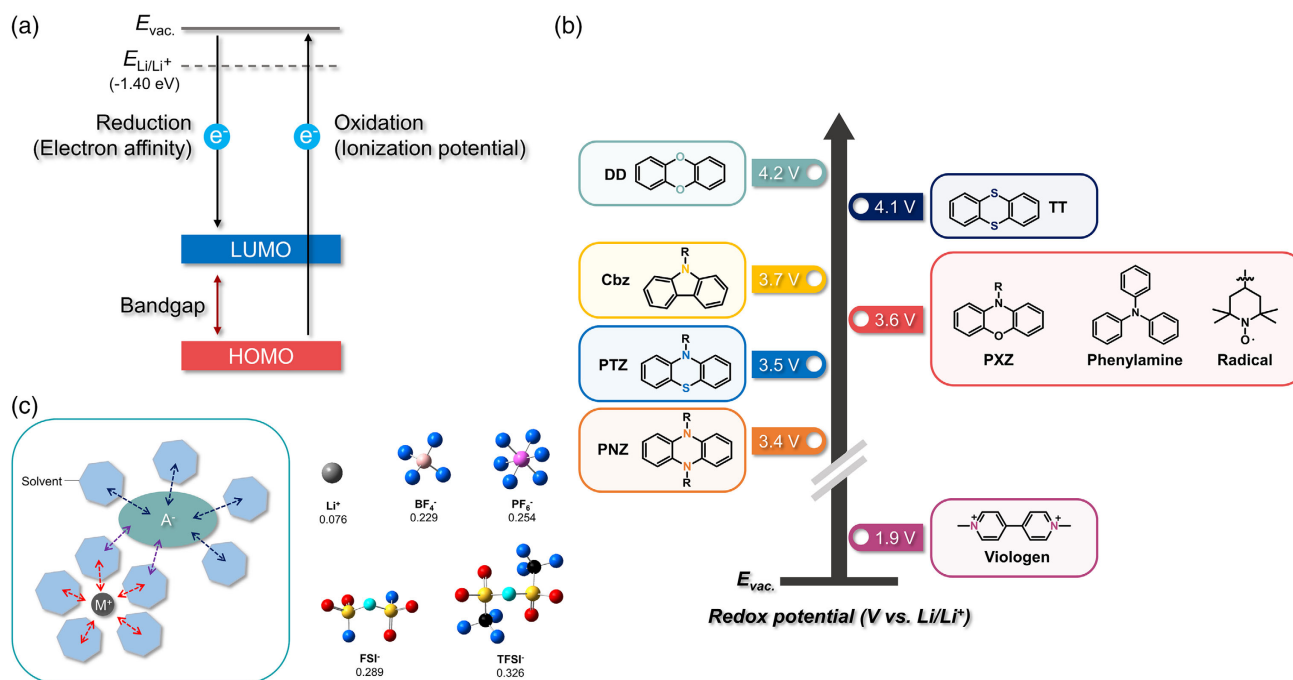

Figure 2. a) The frontier molecular orbitals (FMOs) related to redox reaction of ROMs. b) Various p-type ROMs with their average redox voltage. c) A schematic illustration of a solvated anion and cation in the electrolyte. Comparisons of molecular shape and size (Å) of Li-ion and representative anions.

phenothiazine (PTZ, Section 3.4.2),[88] phenoxazine (PXZ, Section 3.4.3),[89] thianthrene (TT, Section 3.4.4),[90] and dibenzodioxin (DD, Section 3.4.4).[91] Surprisingly, a DD compound showed one of the highest redox potentials ($\approx$4.2 V vs Li/Li$^+$) among the ROMs. In contrast, a unique class of p-type ROMs was reported with much lower redox potential (<2.0 V vs Li/Li$^+$) than the others. Viologens occur in dication with two counter anions, and therefore, they tend to be doubly reduced to form a neutral species (Section 3.6).[32] However, since their redox reactions accompany counter anions rather than metal cations, the viologens are usually classified as p-type ROMs.

2.2. Effect of Counter Anions

As the redox reactions of p-type ROMs involve anion charge compensation, the p-type ROMs are typically suitable for dual-ion[29,30,92] and anion-shuttle batteries[32,93–95] rather than for Li-ion and Li-metal batteries. Such batteries using the anion chemistry have recently emerged due to their potential advantages such as high voltage, large capacity, and fast rate capability. Particularly, in dual-ion batteries, graphite has been studied for a cathode material due to its high voltage (>4.5 V vs Li/Li$^+$) and fast rate capability.[96,97] However, its high working voltage (>4.5 V vs Li/Li$^+$) beyond the electrochemical window of the electrolyte often induces electrolyte decomposition, which can be accelerated by defects in the graphite electrode. Furthermore, the huge volume changes during successive de-/intercalation of bulky anions are harmful for the cycle stability.

In contrast, the p-type ROMs have inherently flexible intermolecular structure that facilitates de-/intercalation of bulky anions. Also, their electrochemical properties such as the redox potential can easily be tailored by proper molecular designs. But, due to the lack of pre-lithiated n-type ROMs stability in the ambient condition, an all-organic battery relying on the metal-ion rocking-chair mechanism is still far from practical. Therefore, we believe p-type ROMs would be a key for achieving a practical all-organic full-cell based on dual-ion and anion rocking-chair mechanisms.

Typically, anions (e.g., BF$_4^-$, PF$_6^-$, FSI$^-$, and TFSI$^-$) are bulkier than metal cations. Thus, the charge is more delocalized over the bulky anion molecules, leading to weak interaction with the solvent molecules and less solvation in the electrolytes. Such features endow the anions with fast diffusion into the electrode materials and rapid ionic conductivity with a high transference number (Figure 2c).[98–100] In a typical battery, the rate capability is determined by i) the diffusion of charge-carrying ions and ii) heterogeneous electron transfer rate (k^0) with iii) electron conductivity of active materials.[101] Therefore, high-rate performance is expected from a battery using the p-type ROMs. However, despite the benefits such as high voltage and rate capability, in practice, most p-type ROMs still exhibit low capacity and, consequently, poor energy density due to irreversible second redox.

Furthermore, although the counter anions in electrolytes play important roles as charge carriers, influence of the shape, size, and concentration on the cell performance is still elusive. In the case of n-type ROMs, it is well known that types of charge-carrying cations (e.g., Li$^+$, Na$^+$, and K$^+$) significantly affect their electrochemical performance including redox voltages, capacity utilization, and cycle stability.[25,27,102–104] However, comparative studies between different charge-carrying anions are scarcely reported for the p-type ROMs. Very recently, a preliminary study showed that the insertion of bulky V-shaped TFSI$^-$ anion exfoliated the organic active materials from the electrode upon cycling, which led to capacity fading.[105] Therefore, designing new p-type ROMs capable of multi-electron redox and garnering insights into the fundamentals of anionic chemistry inside the cells are both imperative.

3. Classification Based on Redox Centers

3.1. CPs

The discovery of highly conducting polyacetylene (PAc) by Alan J. Heeger, Alan G. MacDiarmid, and Hideki Shirakawa in the 1970s proved that organic polymers could be electrically conductive as metals.[106] Subsequently, various CPs, such as PPy,[107] PANI,[108,109] PTh,[110] poly(indole),[111] and polyphenylene (PP),[45] were reported (**Figure 3**). Meanwhile, in the late 1980s, PANI showed promising electrochemical properties as a cathode active material in a Li metal–based secondary battery, which triggered polymer battery research.[43] It was expected that the highly conducting nature of CPs would give them high-rate capability and reduce the use of conductive carbon additives.

However, several shortcomings limited the practical use of CP electrodes. The high electric conductivity of CPs is given by polarons and bipolarons formed along the conjugated backbones upon the p-type doping process. Thus, the energy levels and conductivity of CPs alter by the degree of p-type doping.[112,113] But, in the polymer batteries, the CP electrodes utilized such a p-type doping process (i.e., an oxidation reaction) as a charge storage mechanism. It means that the energy levels (i.e., redox potentials) and conductivity of the CP electrodes continuously change during charge/discharge, bringing about a floating average voltage with a slopy plateau and fluctuating rate performance.[114] Moreover, inefficient doping capability (<50%) with the irreversibility of CPs led to a low specific capacity,[115,116] and their inherent poor solubility also made the electrode fabrication process inconvenient. To avoid such drawbacks in utilizing CPs, Yao group proposed a novel design strategy that is separating the redox centers from the π-conjugated backbone.[117] They demonstrated that P(NDI2OD-T2) polymer delivered 100% of its theoretical specific capacity with a flat voltage plateau. The result was attributed to that the two imide-based n-type redox centers, which were attached to the backbone as a pendant group, could undergo fully reversible two single-electron redox reactions without affecting the energy levels of the backbone. Moreover, the electrons generated/inserted during the redox are assumed to be efficiently transported through the polythiophene-like π-conjugated backbone, leading to superior rate performance.

3.2. Phenylamine Compounds

As a p-type redox center, di- and triphenylamine (TPA) have drawn much attention due to the high stability of the oxidized form (i.e., radical cation) and superior hole-transporting
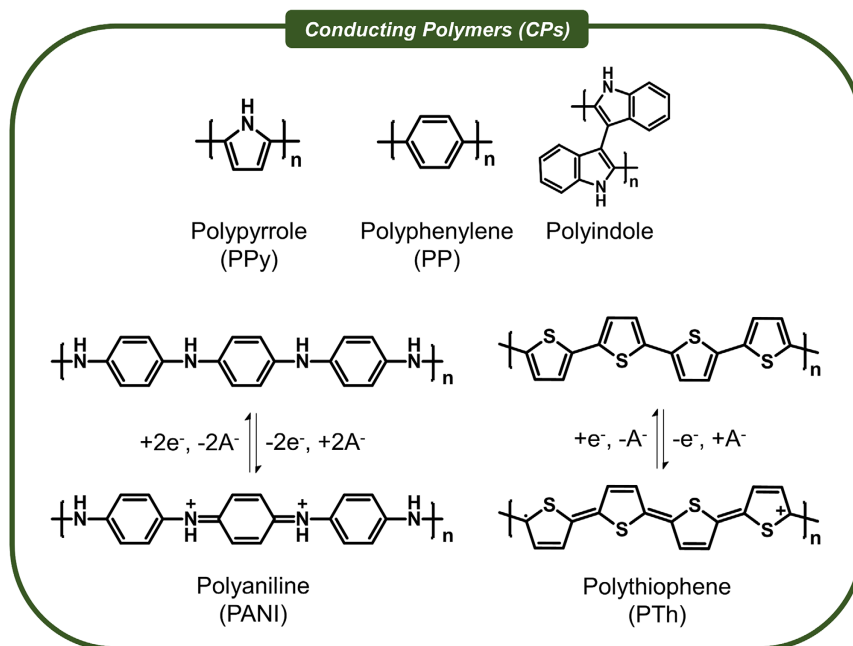
**ADVANCED
SCIENCE NEWS**

www.advancedsciencenews.com

**ADVANCED
ENERGY & SUSTAINABILITY
RESEARCH**
Open Access

www.advenergysustres.com

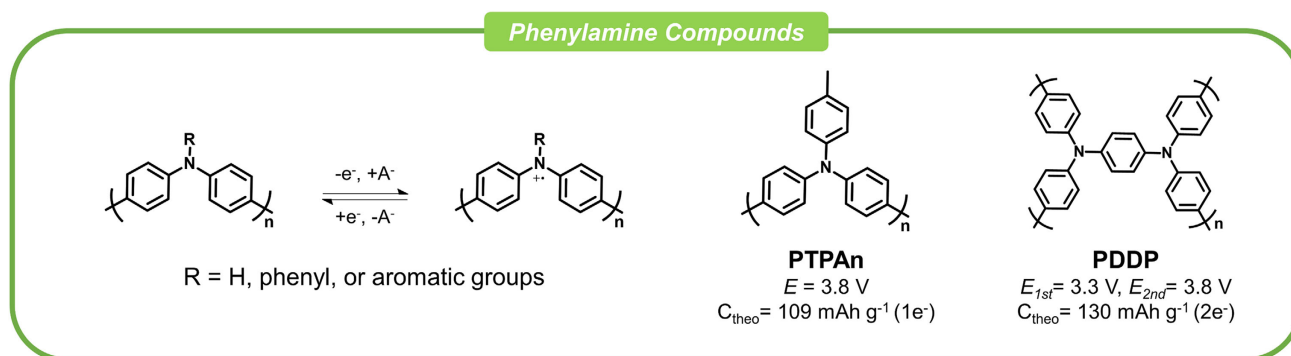**Figure 3.** Molecular structures and the redox mechanism of conducting polymers.

Figure 4. The redox mechanism of phenylamine compounds with representative molecular structures.

properties (**Figure 4**). The two (or three) phenyl rings attached to a central nitrogen atom in the phenylamines effectively stabilize a radical cation formed in their oxidized state. The first phenylamine compound, polytriphenylamine (PTPAn), for a cathode material in a lithium battery was reported in 2008 by Feng et al.[118] The PTPAn electrode delivered a specific capacity of 103 mAh g^{-1} at 0.5C with a well-defined discharge voltage plateau of 3.8 V versus Li/Li$^+$. Interestingly, 90% of the low-rate discharge capacity (91 mAh g^{-1}) was maintained even at 2C, which was attributed to the well-specified redox center with partially π-conjugated structures of the polymer. However, the theoretical specific capacity of PTPAn is only up to 109 mAh g^{-1}, which is notably lower than that of conventional inorganic electrodes. Poly[N,N,N,N-tetraphenylphenylenediamine] (PDDP), which bears two TPA redox centers in a monomeric unit, was subsequently developed to increase the specific capacity.[71] PDDP delivered a higher specific capacity of 129 mAh g^{-1} than PTPAn at the initial cycle with two distinct plateaus at

3.3 and 3.8 V versus Li/Li$^+$. But, the capacity dropped to 110 mAh g^{-1} after 50 cycles, and the rate capability was poorer than PTPAn.

Recently, Filipp et al.[119] developed a diphenylamine-based polymer polydiphenylamine (PDPA) for a cathode material in lithium- and potassium-based dual-ion batteries. Compared to the TPA-based polymers, PDPA has one less phenyl ring in a monomeric unit and thus possesses a higher theoretical capacity up to 160 mAh g^{-1} (**Figure 5**a). In cyclic voltammetry (CV) measurements, PDPA showed two broad anodic peaks at 3.53 and 3.97 V versus Li/Li$^+$, indicating that two electrons were removed from the two phenylamine redox centers in sequence to form a quinonediimine structure upon oxidation. Surprisingly, the use of 10 wt% multiwalled carbon nanotubes (MWCNTs) instead of conventional carbon additive (i.e., Super-P) could significantly increase the PDPA content in the electrode up to 80 wt% without performance deterioration by lowering the charge-transfer (CT) resistance of the electrode. Typically, the inherently low electric
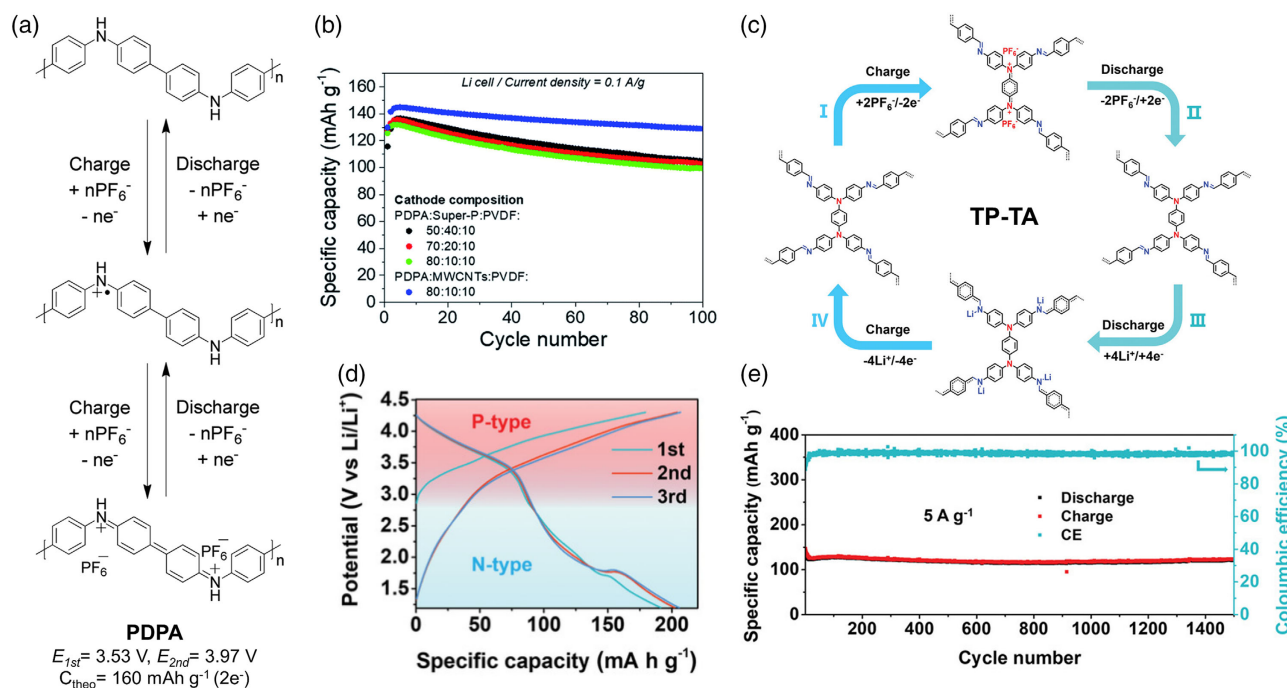
Figure 5. a) Charge/discharge mechanism and molecular structure of PDPA. b) Cycling performance of PDPA at current density of 0.1 A g^{-1}. Reproduced with permission.[119] Copyright 2021, Royal Society of Chemistry. c) The molecular structure and redox mechanism of TP-TA. d) The charge–discharge profiles of phenylenediamine-terephtalaldehyde (TP-TA) in the range of 1.50–4.25 V. e) Long-term cycling test at high current of 5 A g^{-1}. Reproduced with permission.[128] Copyright 2021, Wiley-VCH GmbH.

conductivity makes it difficult to achieve high-capacity utilization in the organic electrodes with the large content of active materials. However, a specific capacity as high as 145 mAh g^{-1} was attained with a 99% of capacity retention after 100 charge/discharge cycles from the PDPA/MWCNTs electrode (Figure 5b). Consequently, in a Li cell, it delivered the highest specific energy of 418 Wh kg^{-1} among phenylamine- and radical-based cathodes when considered by the whole electrode weight. Nevertheless, the capacity drop was observed at a high rate of 1 A g^{-1} in a Li cell. It became severer in a K cell, attributed to the morphological degradation and partial dissolution of PDPA in the electrolyte.

To circumvent such a solubility issue, hyper-cross-linked polymers[120–122] and micro/mesoporous covalent organic frameworks (COFs) have been studied.[70,123–125] In particular, synthesizing COFs effectively suppressed the dissolution of active materials in the electrolyte due to high molecular weight and tight intermolecular interactions, leading to high cycle stability. Nevertheless, several COFs suffer from low utilization of redoxactive sites because tightly stacked layers owing to strong π–π interactions hindered efficient access of counter ions.[126,127]

Chen group synthesized a bipolar-type COF, TP-TA, which possessed both p-type phenylamine and n-type Schiff base redox centers (Figure 5c), using a one-step solvothermal method.[128] With the aid of bipolar-type multi-electron redox (two electrons for p-type and four electrons for n-type, respectively), the TP-TA base COF delivered a high specific capacity up to 207 mAh g^{-1} at 200 mA g^{-1} and retained a capacity of 145 mAh g^{-1} after 250 cycles (Figure 5d). Furthermore, at a high rate of 5 A g^{-1}, a

reversible capacity of 122 mAh g^{-1} was maintained for 1500 cycles (Figure 5e). Such outstanding cycle and rate performance were attributed to that the 3D flower-like morphology of TP-TA, which is assembled by ultrathin 2D hexagonal nanosheets, allowed efficient diffusion of counter ions to the redox centers. Nevertheless, the twice higher capacity contribution (>100 mAh g^{-1}) from the n-type process lowered the average voltage as low as 3 V versus Li/Li$^+$. The phenylamine-based ROMs reported to date have a capacity of less than 150 mAh g^{-1} with a moderate average voltage of 3.6–3.8 V versus Li/Li$^+$. Therefore, developing a new design strategy is necessary to increase both voltage and capacity.

3.3. Dibenzo-Annulated Heterocyclic Five-Membered Ring Compounds

In 1991, Shirota et al.[129] reported that the redox potential of poly(N-vinylcarbazole) (PVK) was not affected by the doping level because the Cbz redox center was attached to the nonconjugated backbone as a pendant group (**Figure 6**a). Based on this idea, Yao et al.[69] evaluated PVK as a cathode for a Li battery to show a voltage plateau at 3.7 V versus Li/Li$^+$ with a discharge capacity of 125 mAh g^{-1}. However, due to the insufficient electrical conductivity of the polyethylene backbone, a large amount of conductive carbon additives (>40 wt%) was required for the electrode. Subsequently, instead of insulating polyvinylidene fluoride (PVDF) binder, Poly(3,4-ethylenedioxythiophene):poly(styrenesulfonate) (PEDOT:PSS) was used to increase conductivity of the electrode film, which led to ultrafast rate performance of
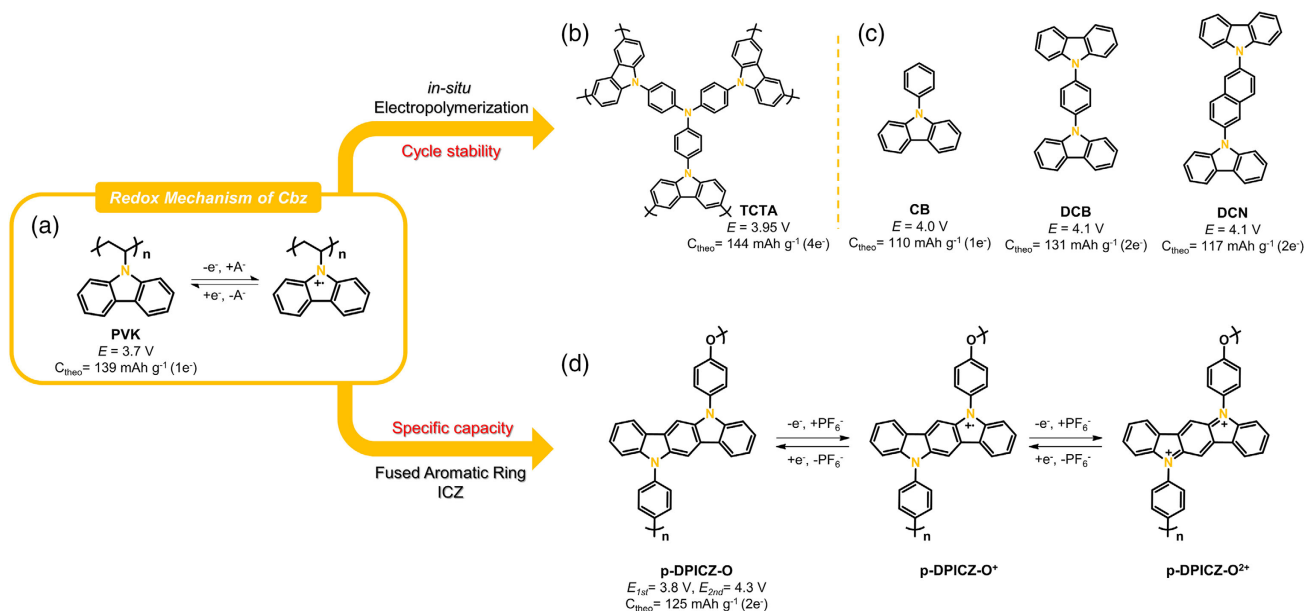
Figure 6. Schematic diagram of the redox mechanism and molecular design strategies for carbazole (Cbz)-based ROMs. a) The redox mechanism of the Cbz redox center. b,c) The chemical structures of monomers for in situ electropolymerization. d) The chemical structures and redox mechanism of indolocarbazole (ICZ)-based polymer (5,11-diphenyl-5,11-dihydroindolo[3,2-b]carbazole) with an ether linkage (p-DPICZ-O).

the PVK electrode.[68] Surprisingly, the PVK electrode with 1.0 wt% of PEDOS:PSS delivered more than $75\,mAh\,g^{-1}$ of specific capacity even at 20C, but it still contained 40 wt% of carbon black.

Dissolution of active materials into the organic electrolytes is a common problem inducing rapid capacity fading.[130] Recently, Zhao et al.[131] developed a Cbz-based small molecule cathode capable of undergoing in situ electropolymerization during cell operation for the first time. The 3- and 6-position of the Cbz redox center become highly reactive in the oxidized state, which results in a cross-coupling reaction to form a Cbz dimer.[132,133] To take advantage of such a dimerization process, 4,4',4''-tris (carbazole-9-yl)-triphenylamine (TCTA) was prepared, in which three Cbz groups attached to a TPA core (Figure 6b). In a few initial cycles, Cbz units underwent dimerization to form network polymers of TCTA at a cutoff voltage of 4.1 V versus Li/Li+. After polymerization, the TCTA electrode delivered a discharge capacity of $92.2\,mAh\,g^{-1}$ with a high average discharge voltage of 3.95 V versus Li/Li+. Furthermore, the polymerization endowed the TCTA electrode with outstanding cycling stability (60% capacity retention for 5000 cycles, **Figure 7**a) and high-rate capability ($38\,mAh\,g^{-1}$ at $20\,A\,g^{-1}$).

Subsequently, a comparative study to find optimal molecular design of the Cbz monomer was reported to improve the performance.[134] Three monomers—9-phenylcarbazole (CB), 1,4-bis (carbazol-9-yl)benzene (DCB), and 2,6-bis(carbazol-9yl) naphthalene (DCN)—were prepared, which had different core sizes and the number of polymerizable sites (see Figure 6c for the molecular structures). The cycling stability of CB was notably lower than the other monomers even after polymerization (**Figure 7**b), which was attributed to that CB could form only a linear polymer with good solubility. In contrast, the four polymerizable sites in DCB and DCN formed network polymers

with poor solubility by in situ polymerization. Interestingly, DCN showed higher capacity retention (76.2% after 5000 cycles) than DCB (68.7%). It was attributed to that the larger size core of DCN facilitated intermolecular interactions, leading to lower solubility. Nevertheless, the specific capacities delivered by the electropolymerized Cbz-based cathode were limited below $100\,mAh\,g^{-1}$, because the Cbz redox center could undergo only one single-electron redox reaction.

To increase the specific capacity, an indolocarbazole (ICZ) redox center bearing two Cbzs, fused by a benzene ring, was reported (Figure 6d).[135] Because it has two Cbz units, ICZ-based electrodes were expected to have a higher specific capacity than the Cbz derivatives. Dai et al. synthesized an ICZ-based polymer p-DPICZ-O by introducing a flexible ether linkage to facilitate anion diffusion into the polymer structures. As expected, the p-DPICZ-O electrode showed two distinct plateaus at 3.8 and 4.3 V versus Li/Li+, respectively; however, its practical specific capacity was only $90\,mAh\,g^{-1}$, which corresponds to 72% of its theoretical capacity (Figure 7c,d). Nevertheless, it showed one of the highest redox potentials among the p-type ROMs due to more diluted electron density, particularly compared with the dibenzo-annulated heterocyclic six-membered ring redox centers, which will be discussed in the next section.

3.4. Dibenzo-Annulated Heterocyclic Six-Membered Ring Compounds

As mentioned earlier, the Cbz derivatives showed promisingly high redox potentials, but their specific capacities were mostly below $100\,mAh\,g^{-1}$. Such low capacities are attributed to the fact that the Cbz unit undergoes a single-electron redox reaction relying on only one nitrogen heteroatomic redox center. Therefore,
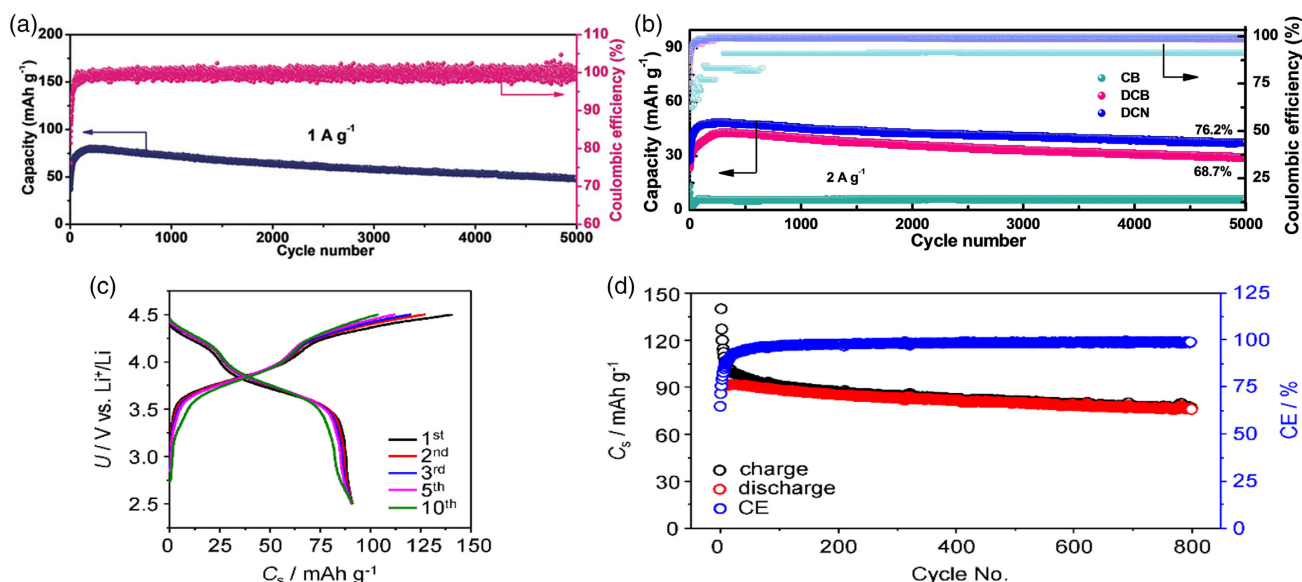
ADVANCED
SCIENCE NEWS
www.advancedsciencenews.com

ADVANCED
ENERGY & SUSTAINABILITY
RESEARCH
Open Access
www.advenergysustres.com

Figure 7. a) Long-term cycling stability test of 4,4′,4″-tris(carbazole-9-yl)-triphenylamine (TCTA) up to 5000 cycles at a current density of 1 A g^{-1}. Reproduced with permission.[131] Copyright 2020, Wiley-VCH GmbH. b) Long-term cycling test of 9-phenylcarbazole (CB), 1,4-bis(carbazol-9-yl)benzene (DCB), and 2,6-bis(carbazol-9yl)naphthalene (DCN) at a current density of 2 A g^{-1} after in situ electropolymerization. Reproduced with permission.[134] Copyright 2021, Wiley-VCH GmbH. c) Charge–discharge profiles of p-DPICZ-O at a current density of 1C. d) Cycling performance of p-DPICZ-O for 800 cycles. Reproduced with permission.[135] Copyright 2020, European Chemistry Societies Publishing.

in recent years, increasing attention has been paid to p-type ROMs capable of multi-electron redox reactions for achieving a large capacity. In particular, several research groups have focused on a series of dibenzo-annulated heteroaromatic six-membered rings, such as dihydrophenazine (PZ), PTZ, PXZ, TT, and DD, as a new multi-electron ROM (**Figure 8**). Such ROMs bear two heteroatomic redox centers (i.e., N, S, and O) in the core six-membered ring, which is fused by two respective benzene rings. Thus, they are typically able to undergo two single-electron redox reactions to have a considerably higher theoretical specific capacity ($\approx$270 mAh g^{-1}) than Cbz. Interestingly, their redox potentials substantially vary from 3.1 to 4.2 V versus Li/Li$^+$ depending on the electron-donating/withdrawing strength of heteroatoms.

Conventionally, due to the reversible redox reaction and stable oxidized state, they have been used as a functional group in many organic semiconductors for hole-transporting materials,[136–138] electrochromic materials,[139,140] electro-/photoluminescence materials,[141–144] photocatalyst,[145–147] and redox mediators.[148–150] In addition, taking advantage of a high redox potential, they have been successfully utilized as a redox shuttle for high-voltage LIBs.[151,152]

In the following sections, we review the recent research progress of each dibenzo-annulated hexatomic ring redox centers and introduce detailed molecular design strategies to improve their electrochemical performance in secondary batteries.

3.4.1. PZ

In 2017, Lee et al.[65] first employed dimethylphenazine (DMPZ) as a new p-type multi-electron redox ROM (**Figure 9**a). The

DMPZ electrode showed two well-defined plateaus at 3.1 and 3.7 V versus Li/Li$^+$ and delivered a discharge specific capacity of 191 mAh g^{-1} in the initial cycle. However, the high solubility of DMPZ in the doubly oxidized state (i.e., DMPZ^{2+}) led to severe capacity fading. Subsequently, various strategies have been reported to prevent dissolution (Figure 9b), such as polymerization[66,67,153] and salification.[154] In particular, synthesizing linear polymers of diaryl-PZ effectively suppressed the solubility, and thus the polymer cathodes delivered specific capacities of around 150 mAh g^{-1} with superior capacity retention (>90%) over a few hundred cycles.[66,67,153] However, the strong π–π interactions between the polymer chains narrowed the internal free volume, which adversely affected the rate performance by limiting the diffusion of bulky anions.

To address the rate performance issue, Abruña et al. developed a network polymer of PZ by introducing a phenylene linker (Ph), 135Ph, with three connectivity (Figure 9c).[155] The amorphous nature of the network polymer poly(135Ph-PZ) facilitated surface-controlled kinetics (**Figure 10**a,b), enabling faster ion diffusion (anion diffusion coefficient ($D_{PF6}-$): 9×10^{-9} cm^2 s^{-1}) than a crystalline linear polymer poly(Ph-PZ) (anion diffusion coefficient: 5×10^{-14}–3×10^{-11} cm^2 s^{-1}). Such improved kinetics of poly(135Ph-PZ) led to higher rate performance.[156] At a rate of 1 A g^{-1}, poly(Ph-PZ) delivered a higher specific capacity (193 mAh g^{-1}) than the network polymer poly(135Ph-PZ) (184 mAh g^{-1}). But, when the rate was raised to 16 A g^{-1}, the network polymer could retain more capacity than the linear polymer (138 vs 130 mAh g^{-1}, respectively), indicating higher rate performance of the network polymer. Nevertheless, at a low rate, the capacity utilization of the network polymer (79% of theoretical capacity) was poorer than the linear one (92%). Furthermore, it became worse when increasing the active
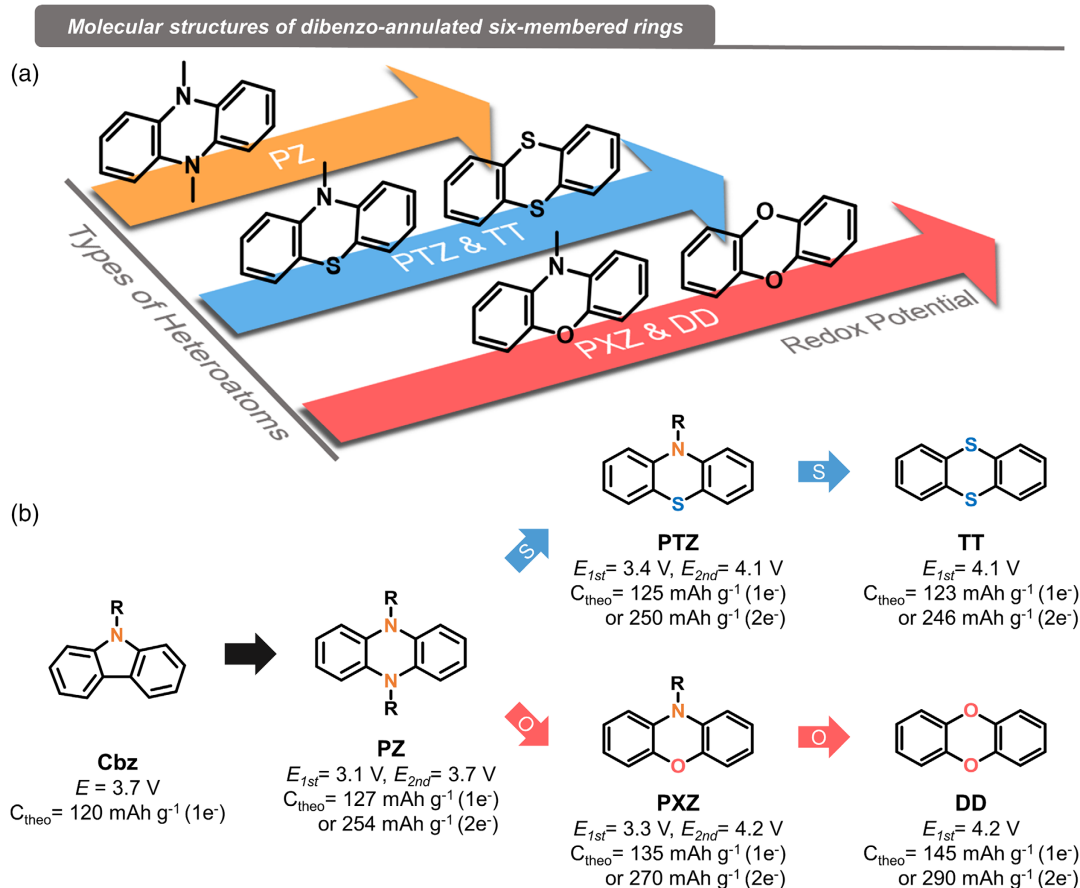
Figure 8. a) Schematic illustration of relationship between the redox potential and heteroatoms in the dibenzo-annulated six-membered rings. b) The chemical structures with redox potential (vs Li/Li$^+$) and theoretical specific capacity of the dibenzo-annulated six-membered ring compounds.
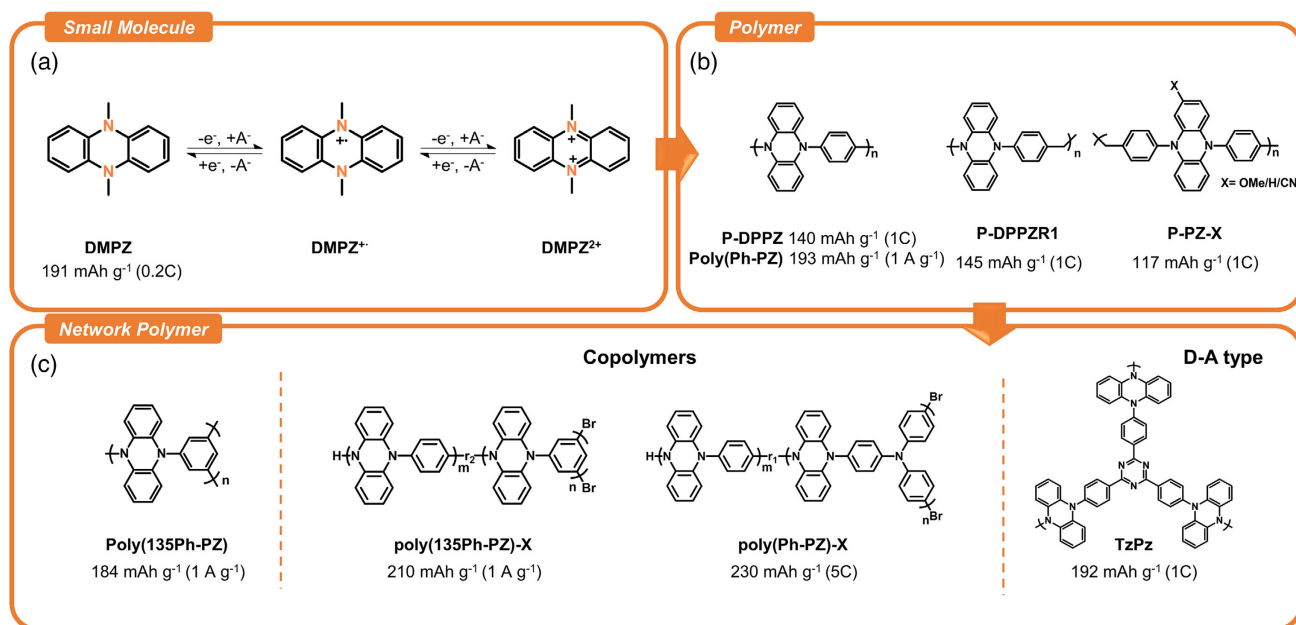

Figure 9. a) The redox mechanism and chemical structure of a phenazine-based model compound, dimethylphenazine (DMPZ). The chemical structures of phenazine-based b) polymers and c) network polymers. Although poly(*N,N'*-diphenyl-5,10-dihydrophenazine) (P-DPPZ)[153] and poly(Ph-PZ)[156] have the same molecular structure, they are differently reported in the two papers. The practical capacities are shown with the corresponding C-rates.
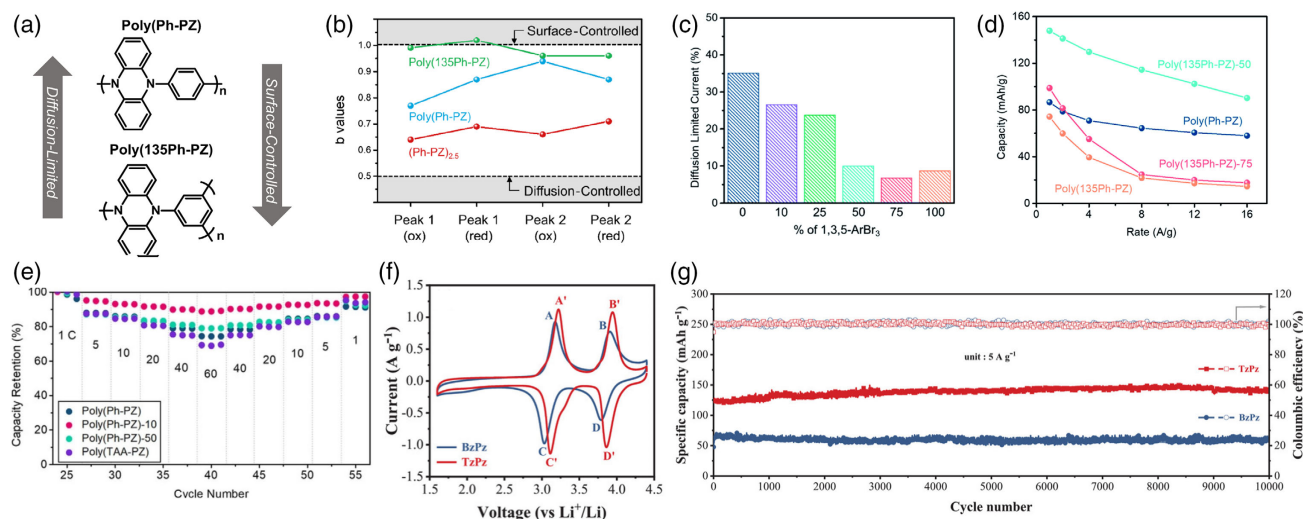
**ADVANCED
SCIENCE NEWS**

www.advancedsciencenews.com

**ADVANCED
ENERGY & SUSTAINABILITY
RESEARCH**
Open Access

www.advenergysustres.com

Figure 10. a) Charge storage mechanism difference between (Ph-PZ) (top) and poly(135Ph-PZ) (bottom) depending on the crystallinity. b) The *b* values of the oligomer (Ph-PZ)$_{2.5}$, the linear polymer poly(Ph-PZ), and the network polymer poly(135Ph-PZ). Reproduced with permission.[155] Copyright 2021, American Chemical Society. c) The portions of diffusion-limited current for poly(135Ph-PZ)-X with different molar ratios of network linker (1,3,5-ArBr$_3$). d) The specific capacity of poly(Ph-PZ) and poly(135Ph-PZ)-X depending on C-rate with 80% of active materials in the electrode. Reproduced with permission.[156] Copyright 2021, Royal Society of Chemistry. e) The rate capability of poly(Ph-PZ)-X at current density of 1 to 6C. Reproduced with permission.[157] Copyright 2020, Wiley-VCH GmbH. f) Cyclic voltammograms of BzPz and TzPz at a scan rate of 1 mV s^{-1}. g) Cycling stability measurement of BzPz and TzPz at a current density of 5 A g^{-1} for 10 000 cycles. Reproduced with permission.[158] Copyright 2021, Wiley-VCH GmbH.

content in the electrode from 60 to 80 wt%, which was due to the higher charge transport resistance of the network polymer.

To compromise between such ionic- and electronic-preferable conductivity of the two polymers, Gannett et al. synthesized a series of copolymers with different ratios of the linear and network linkers (see poly(135-PZ)-X in Figure 9c).[156] Interestingly, depending on the linker ratios, the crystallinity of the copolymers gradually varied, leading to changes in the ion diffusivity and the charge-transfer resistance (Figure 10c). Among the copolymers, poly(135Ph-PZ)-50, which possessed a 50–50% blend ratio, exhibited the highest performance due to optimal characteristics. As a result, the polymer electrode delivered a specific capacity up to 135 mAh g^{-1} at 1.0 A g^{-1} even with 80 wt% of active content, and 65% of the low-rate capacity was retained at a high rate of 16 A g^{-1} (Figure 10d). Then, to increase specific capacity further, Gannett and coworkers substituted the phenylene network linker (i.e., 135Ph) with a TPA group, which could undergo a single-electron oxidation as an additional redox center (see poly(Ph-PZ)-X in Figure 9c).[157] In this case, the optimal comonomer ratio was different from the previous study (Figure 10e). With the aid of an additional redox from the TPA linker, the poly(Ph-PZ)-10 exhibited exceptionally high rate performance with a large capacity; even at 12C rate, a specific capacity of 220 mAh g^{-1} could be delivered by the polymer electrode.

Meanwhile, Wenyan et al. reported a donor–acceptor D–A)-type network polymer, TzPz, containing PZ and triazine (Tz) units as an electron donor and acceptor, respectively (Figure 9c).[158] As expected, the electron-withdrawing effect of the Tz unit elevated the redox potential of TzPz compared to its counterpart polymer BzPz possessing a benzene core instead of Tz (Figure 10f). Furthermore, the push–pull structure of TzPz

enhanced the conjugation degree and narrowed the bandgap, leading to better rate performance than BzPz by facilitating charge transport. Finally, outstanding cycle stability over 10 000 cycles was achieved from the TzPz electrode (Figure 10g).

3.4.2. PTZ

PTZ, an analogue of PZ, has a sulfur/nitrogen heteroatom pair in the six-membered core ring. It is one of the naturally occurring antioxidants, and its derivatives have widely been used for pharmaceuticals due to its high bioactivity.[159,160] As mentioned in Section 3.4 (vide supra), substituting a nitrogen atom of PZ by sulfur leads to elevation of the redox potential due to weaker electron-donating strength.[161]

In 2017, Kolek et al.[88] reported a PTZ-based polymer PVMPT, in which *N*-methylated PTZ (MPT) units were attached to a vinyl backbone as a pendant group, for an organic cathode material (**Figure 11**). In the polymer, each MPT unit underwent two single-electron oxidations in a stepwise manner at 3.44 V (the neutral state **A** to the radical cation state **C**) and 4.18 V versus Li/Li$^+$ (to the dicationic state **D**), respectively. As expected, the redox potentials of PVMPT were much higher than those of DMPZ (vide supra). Interestingly, in the CV measurements, it was found that oxidation of PVMPT imposed strong π–π interactions between the neighboring MPT dimers, leading to the occurrence of the intermediate oxidation state **B** (Figure 11a). Such strong interactions stabilized the oxidation states **B** and **C**, providing exceptionally high cycle stability (93.5% capacity retention after 10 000 cycles) and rate capability (46% capacity retention at 10C) (**Figure 12**a,b). However, due to such strong interactions, a complete reduction of PVMPT back to the neutral
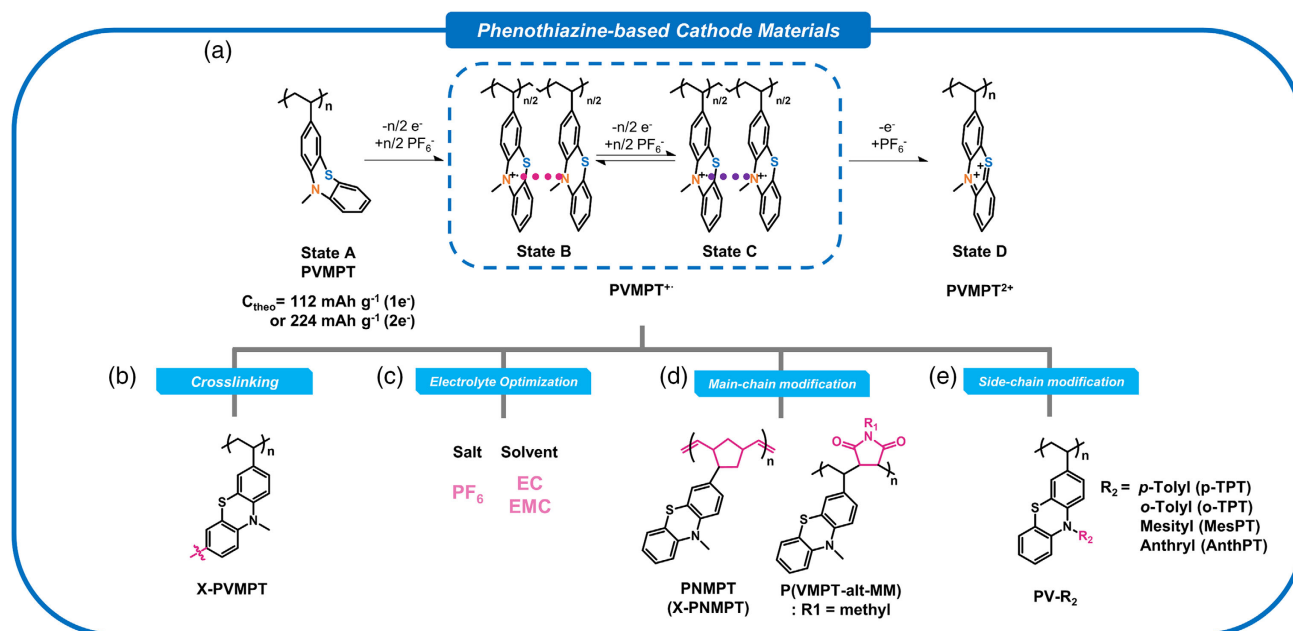
Figure 11. a) The chemical structure and the redox mechanism of poly(3-vinyl-*N*-methylphenothiazine (PVMPT)). b–e) Molecular design strategies to improve the electrochemical performance of PVMPT.
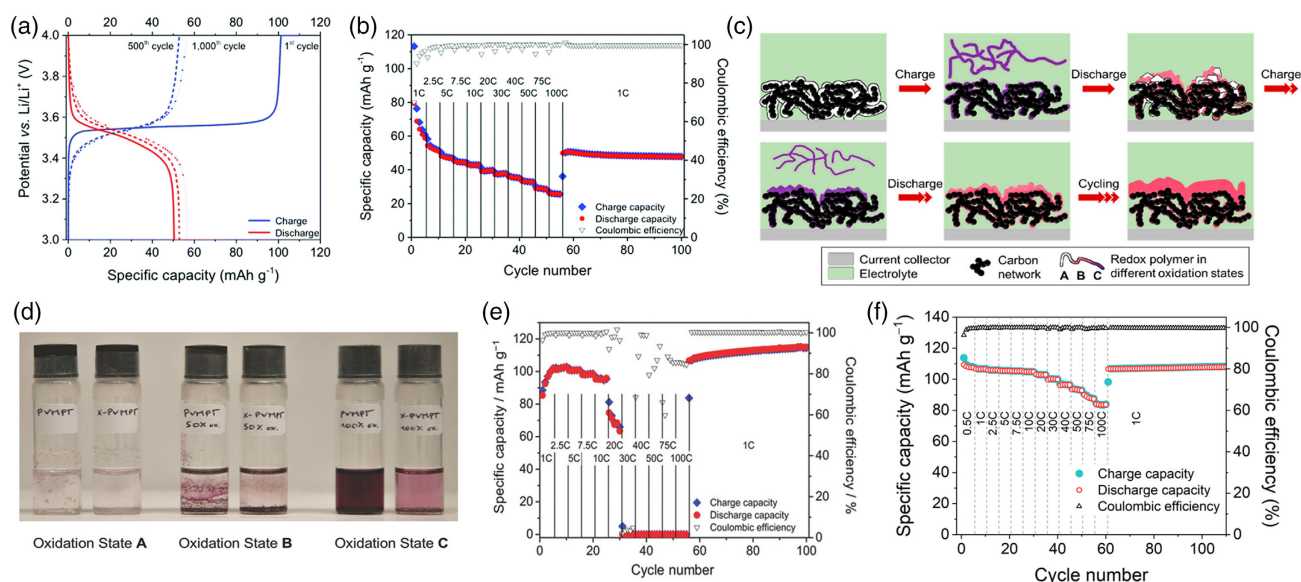

Figure 12. a) Galvanostatic charge–discharge profiles of PVMPT at 1C over 500 cycles and b) its rate capability test up to 10C. Reproduced with permission.[88] Copyright 2017, Royal Society of Chemistry. c) The stabilization process of PVMPT by repeated dissolution/re-deposition during charge/discharge. Reproduced with permission.[162] Copyright 2018, American Chemical Society. d) Solubility test of PVMPT and X-PVMPT in ethylene carbonate (EC):dimethyl carbonate (DMC) (1:1) with 1 M LiPF$_6$ in the neutral and oxidation (50%, 100%) states. e) The rate capability measurement for X-PVMPT up to 10C. Reproduced with permission.[163] Copyright 2018, Wiley-VCH GmbH. f) The rate capability test of the original PVMPT in the optimal electrolyte (EC:ethyl methyl carbonate (EMC) (3:7) with 1 M LiPF$_6$). Reproduced with permission.[164] Copyright 2021, American Chemical Society.

state **A** was prohibited. In addition, the second oxidation of the MPT unit to form the oxidation state **D** was revealed to be partially irreversible, significantly degrading the cycle stability. As a result, the maximum reversible specific capacity of PVMPT was limited up to 56 mAh g^{-1} that corresponds to only a half-electron utilization (theoretical capacity = 112 and

224 mAh g^{-1} for one- and two-electron utilization, respectively). A subsequent study revealed that the dissolution of PVMPT upon oxidation activated the stabilization process through rearrangement of the polymer chains. The repeated dissolution/re-deposition during the successive charge/discharge formed ionically and electronically conductive polymer films, which

**ADVANCED
SCIENCE NEWS**

www.advancedsciencenews.com

**ADVANCED
ENERGY & SUSTAINABILITY
RESEARCH**
Open Access

www.advenergysustres.com

led to such high cycle and rate performance, sacrificing the specific capacity (Figure 12c).[162]

Then, the same research group attempted to suppress the dissolution of the polymer by cross-linking the polymer chains[163] or optimizing the electrolyte (Figure 11b,c).[164] First, the cross-linked polymer X-PVMPT was prepared by introducing a comonomer bearing divinyl moiety.[163] Suppression of the rearrangement process due to insolubility (Figure 12d) allowed X-PVMPT to access the full one-electron oxidation between the states **A** and **C**, leading to an increase in its specific capacity up to 112 mAh g^{-1}. However, it cost the rate capability of the polymer; X-PVMPT was able to deliver a negligible specific capacity at faster rates than 2C (Figure 12e). In contrast, changing the electrolyte solvent mixture from EC:DMC (1:1) to EC:EMC (3:7) also allowed the original PVMPT polymer to access its full capacity by hindering the dissolution but without deterioration of the rate capability (Figure 12f).[164]

To gain more insight into the dimer interaction of PTZ, Esser et al. applied two different molecular design strategies to the PVMPT polymer. One is changing the polymer backbone from vinyl to bulkier, such as norbornene (PNMPT)[165] and methyl-maleimide (P(VMPT-alt-MM)) (see the chemical structures in Figure 11d).[166] The other is introducing a bulky substituent into the N-position of the PTZ unit (PV-p-TPT, PV-o-TPT, PVMesPT, and PVAnthPT in Figure 11e).[166] Such a series of studies clearly showed that the small changes in the chemical structure of ROMs could considerably influence the electrochemical performance by modulating the supramolecular interactions. Meanwhile, several other papers reporting PTZ-based electrode materials have also been published. In those papers, design strategies such as incorporation into π-conjugated polymers[167,168] and salification[169] were proposed to achieve high performance.

3.4.3. PXZ

PXZ, another analogue of PZ, consists of an oxygen/nitrogen pair in the core ring (**Figure 13**a). Otteny et al.[89] replaced the MPT unit in the PVMPT polymer by N-methylphenoxazine (MPO) to prepare a poly(3-vinyl-N-methylphenoxazine) (PVMPO) polymer

(Figure 13b). In the CV profile, the PVMPO electrode showed two single-electron oxidation reactions at 3.35 and 4.22 V versus Li/Li$^+$. But, as similar as PVMPT, the second reaction was not completely reversible. In sharp contrast to PVMPT, the cycle stability of PVMPO was inferior due to the absence of the π–π interactions between the MPO dimers. However, the cross-linked polymer X-PVMPO showed improved cycle stability by preventing dissolution. The maximum specific capacity delivered by X-PVMPO was as high as 115 mAh g^{-1}, which was close to its theoretical capacity considering a single-electron oxidation (120 mAh g^{-1}). Interestingly, the X-PVMPO cathode retained a specific capacity of 96 mAh g^{-1} at even a very high rate of 10C with superior cycle stability (**Figure 14**a). The authors hypothetically ascribed the higher rate of X-PVMPO than X-PVMPT to more minor geometry changes during the redox reactions and weaker intermolecular interactions.

To compare the electrochemical properties of PTZ- and PXZ-based ROMs, Lee et al.[170] prepared two trimers of PXZ and PTZ (i.e., 3PXZ and 3PTZ, respectively; see Figure 13c and 14e for their chemical structures). In the CV measurements (Figure 14b,c), 3PTZ showed three serial single-electron oxidation curves, indicating that each PTZ unit underwent the first oxidation reaction sequentially. In contrast, it appeared that 3PXZ underwent multi-electron reactions in a different fashion: a two-electron oxidation occurred first, followed by a single-electron oxidation. Such an apparent [2 + 1] redox of 3PXZ led to a much narrower peak separation (344 mV) between cathodic and anodic currents than 3PTZ (677 mV), indicating faster redox kinetics of 3PXZ. The density-functional theory (DFT) calculations revealed that the occurrence of a direct two-electron oxidation from the neutral to the +2 state was preferred in 3PXZ due to negligible structural changes between the two states (Figure 14e). Most importantly, it should be noted that such faster kinetics led to higher rate performance of 3PXZ electrode than 3PTZ in the realistic Li-organic coin cells. The 3PXZ electrode exhibited 73% capacity retention at a high rate of 2C (Figure 14d). However, its maximum specific capacity was still limited up to 112 mAh g^{-1} because the second oxidation of each PXZ unit was not accessible.
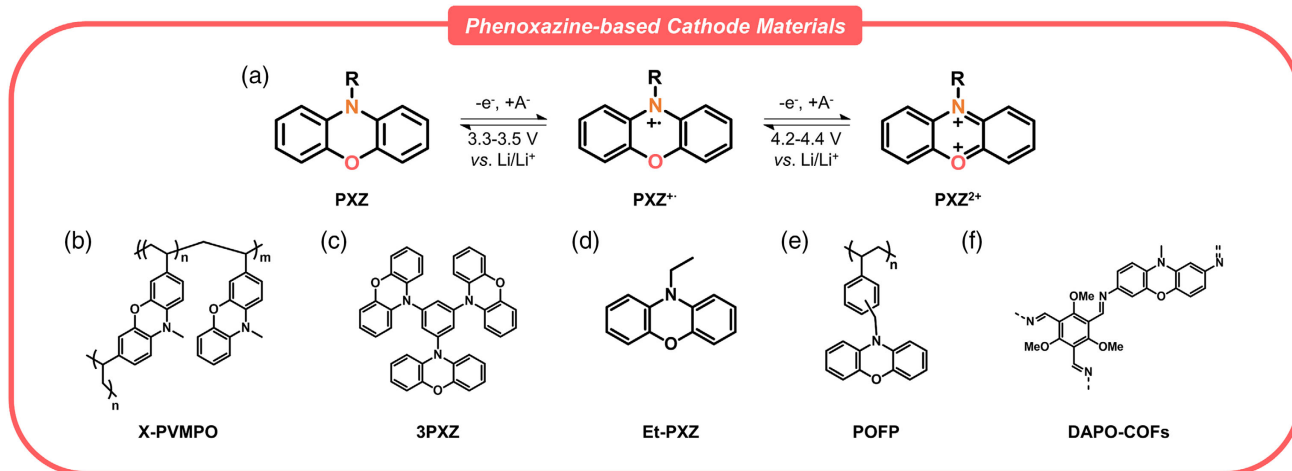

Figure 13. a) The redox mechanism of the phenoxazine (PXZ) redox center and b–f) the molecular structures of PXZ-based ROMs.
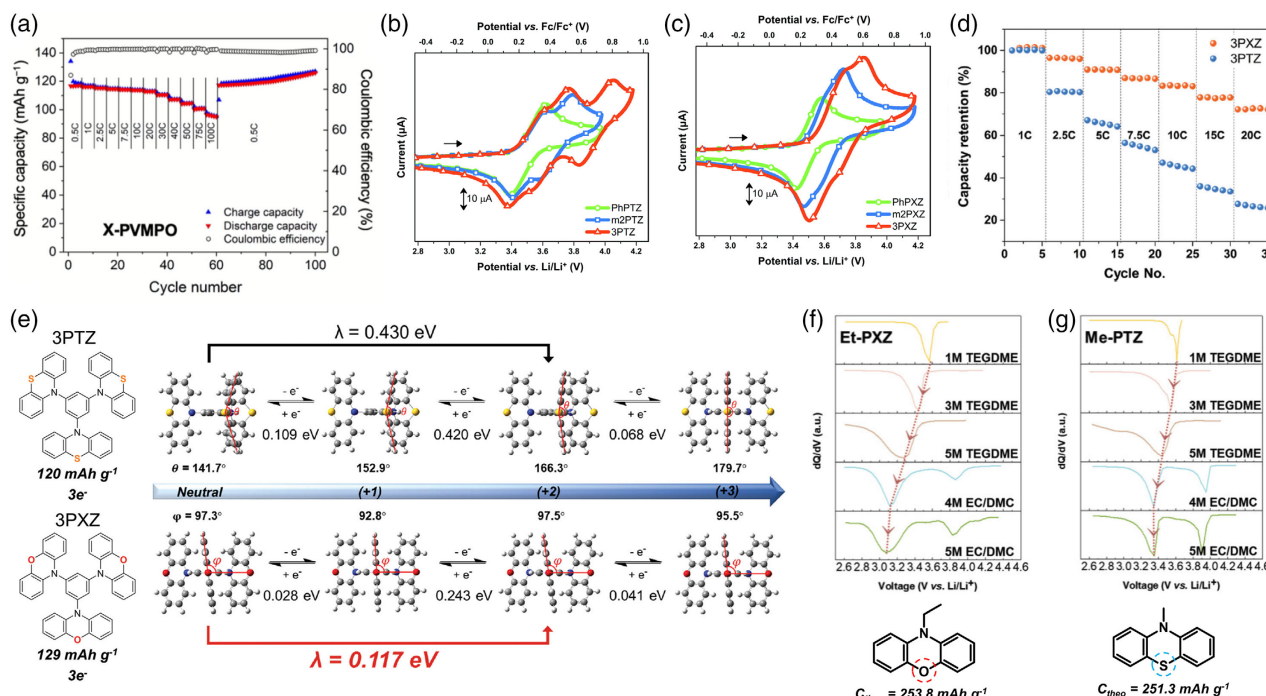
Figure 14. a) The rate performance of the X-PVMPO electrode. Reproduced with permission.[89] Copyright 2019, American Chemical Society. b–d) Electrochemical measurement of phenothiazine (3PTZ) and 3PXZ. Cyclic voltammograms of b) 3PTZ and c) 3PXZ at a scan rate of 100 mV s^{-1}. d) The rate capability measurement from 1C to 2C. e) The optimized geometries of 3PTZ and 3PXZ according to the oxidation states calculated by density-functional theory (DFT). Reproduced with permission.[170] Copyright 2021, Royal Society of Chemistry. The redox potential changes of f) Et-PXZ and g) Me-PTZ by varying the electrolyte. Reproduced with permission.[161] Copyright 2020, Wiley-VCH GmbH.

The reversible access to the second oxidation of PTZ and PXZ-based ROMs was achieved by optimizing the electrolyte.[161] As shown in Figure 14f,g, 10-ethyl-10H-PXZ (Et-PXZ) and 10-methyl-10H-PTZ (Me-PTZ) were prepared for cathode materials by Lee and colleagues. They attributed the irreversibility of the second redox reaction to the occurrence at high voltages beyond the electrochemical window of the electrolyte. Changing the solvent from tetraethyleneglycol dimethylether (TEGDME) to EC/DMC with a lower donor number and increasing the salt concentration to 5 M successfully placed the second oxidation within the stable electrolyte window. As a result, the Et-PXZ and Me-PTZ electrode showed two distinct plateaus at 3.17/3.82 and 3.35/3.95 V versus Li/Li$^+$ (Figure 14f,g), respectively, which were ≈0.5 V higher than those of DMPZ in the same electrolyte condition. Still, full capacity utilization with stable cyclability was only achieved from their single-walled nanotube (SWNT) composite electrodes (244.2 and 184.9 mAh g^{-1} for Et-PXZ/SWNT and Me-PTZ/SWNT, respectively).[171] Recently, Zhang et al.[171] introduced a more convenient method to prepare a PXZ-based polymer poly(10-(vinylbenzyl)-10H-phenoxazine (POEP)) (Figure 13e). Meng and co-workers[172] also prepared two COF materials bearing the PXZ redox centers (Figure 13f). Those materials showed excellent cycle stability and rate performance with high redox potentials at around 3.6 V versus Li/Li$^+$.

3.4.4. TT and DD

TT and DD are two analogues of PZ, whose two nitrogen atoms in the core six-membered ring are both identically substituted by

either S or O atoms, respectively (**Figure 15**a). Due to the substitution, the two ROMs typically show the highest redox potentials among the family of PZ.

In 2015, three norbornene polymers (**P1–P3** in Figure 15b) bearing one or two TT pendant groups were first reported for organic cathodes by Speer and colleagues.[90] The first oxidation of the polymers showed a high redox potential (≈4.1 V vs Li/Li$^+$), but the second one was irreversible under ambient conditions. The utilization of only one electron limited their theoretical specific capacity to 73 mAh g^{-1}, but in practice, they delivered a specific capacity of ≈66 mAh g^{-1}, which rapidly decayed over 100 cycles (Figure 15c). To increase the specific capacity of the TT-based polymers, Wild et al.[28] changed the backbone from norbornene to vinyl (theoretical specific capacity = 110 mAh g^{-1}). Optimizing the polymerization condition, such as types of solvent and initiator concentration, could increase the molecular weight to prepare insoluble poly(vinylthianthrene) (the polymer **3g** in Figure 15b). The **3g** polymer electrode delivered a specific capacity of 105 mAh g^{-1} at 1C in the initial cycle and retained 86 mAh g^{-1} of a specific capacity after 250 cycles (Figure 15d). Interestingly, even at a high rate of 5C, 86% (≈96 mAh g^{-1}) of its theoretical specific capacity was acquired. By taking advantage of the high voltage and cycle stability, they prepared a dual-ion type all-organic battery coupled with an n-type ROM poly(2-vinyl-tetracyano-9,10-anthraquinonedimethane (TCAQ).[173] The all-organic battery delivered a specific capacity of 105 mAh g^{-1} at 1C with a discharge plateau at 1.35 V.

Meanwhile, Lee et al.[91] identified that DD bearing two oxygen atoms in the hexatomic core ring (see Figure 15a for the chemical
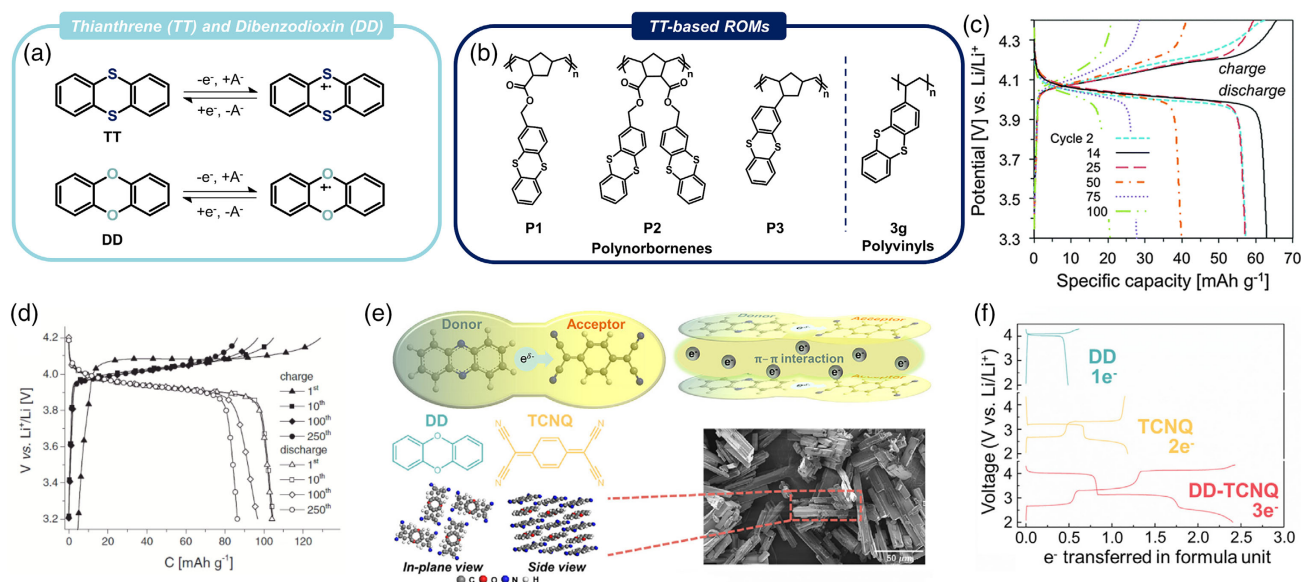
**ADVANCED
SCIENCE NEWS**

www.advancedsciencenews.com

**ADVANCED
ENERGY & SUSTAINABILITY
RESEARCH**
Open Access

www.advenergysustres.com

Figure 15. a) The chemical structures and redox mechanism of thianthrene (TT) and dibenzodioxin (DD). b) The chemical structures of TT-based polymers. c) Charge–discharge profiles of the P1 electrode at 1C. Reproduced with permission.[90] Copyright 2015, Royal Society of Chemistry. d) Charge–discharge curves of **3g**-based electrode at 1C. Reproduced with permission.[29] Copyright 2016, Wiley-VCH GmbH. e) Schematic illustration of the DD–tetracyanoquinodimethane (TCNQ) charge-transfer (CT) complex with a scanning electron microscope (SEM) image of the powder. f) Galvanostatic charge/discharge profiles of the pristine DD and TCNQ electrode and the CT complex electrode at current density of 50 mA g^{-1}. Reproduced with permission.[91] Copyright 2019, Elsevier.

structure) showed its first oxidation at 4.2 V versus Li/Li$^+$, which is slightly higher than TT. To prevent the dissolution of active materials, a CT complex of DD was prepared with tetracyanoquinodimethane (TCNQ) (Figure 15e). The DD–TCNQ complex had lower solubility than the pristine DD and TCNQ molecules due to strong π–π interactions and Coulombic attraction between the layers of DD and TCNQ. Furthermore, the CT complex exhibited considerably higher electric conductivity ($\approx 2.79 \times 10^{-7}$ S cm^{-1}) than that of each pristine molecule due to the partial CT. As the TCNQ molecule was able to undergo n-type redox reactions with two electrons, the DD–TCNQ could utilize three electrons in total (i.e., one electron from a p-type DD molecule and two electrons from an n-type TCNQ molecule, respectively). As a result, the DD–TCNQ electrode delivered a specific capacity of around 170 mAh g^{-1} at 50 mA g^{-1} in the range of 2.6–4.2 V (Figure 15f). Nevertheless, due to a large portion of the specific capacity coming from the n-type reactions, the average charge/discharge voltage of the complex was unexpectedly low. Therefore, it is still required to find a way to utilize the second oxidation of DD- and TT-based ROMs for achieving high energy density.

3.5. Nitroxide Radical Compounds

Since its first report by Nakahara et al. in 2002,[46] the nitroxide radicals have been drawing much attention as a promising ROM due to high voltage, fast kinetics, and large capacity.[174,175,176,177] Among various nitroxides such as proxyl,[174,175] nitroxylbenzene,[50] and nitronylnitroxyl,[178,179] a polymer poly(2,2,6,6-tetramethylpiperidinyloxy-4-ylmethacrylate (PTMA)) bearing a

TEMPO radical pendant group[180,181] has most widely been studied to date (**Figure 16**b,c). The TEMPO radical in PTMA typically shows bipolar type redox: one-electron oxidation (p-type) to form an oxoammonium salt and one-electron reduction (n-type) to form an aminoxyl salt at around 3.5 and 2.8 V versus Li/Li$^+$, respectively (Figure 16a). Each redox process of PTMA theoretically can deliver a specific capacity of up to 111 mAh g^{-1} (i.e., 222 mAh g^{-1} in total). Since the nitroxide-based ROMs have already been comprehensively reviewed by several groups in various point of view,[48,114,174,175,182–186] only a few recent studies focusing on nanocarbon composites are introduced in this section.

Despite enormous efforts, PTMA still suffers from low electrical conductivity and high solubility, which limits its practical use in rechargeable batteries. To circumvent such problems, several strategies have been proposed, including cross-linking the polymer,[51,187] changing the backbone to conjugated framework,[188,189] and physically mixing[180,190–193] or chemically grafting with nanocarbon materials.[194–196] Recently, Zhou et al.[197] fabricated PTMA-grafted MWNT composites (MWNT-g-PTMAs) by a facile in situ polymerization method (**Figure 17**a). The MWNT-g-PTMAs were prepared by the following two steps: first, free radical polymerization of the precursor monomer 2,2,6,6-tetramethylpiperidin-4-yl methacrylate (TMPM) with the acid-treated MWNT, followed by oxidation to form nitroxide radicals. The grafted PTMA content in the composites was conveniently modulated from 26.5% to 41.7% (**MWNT-g-PTMA1–3**). Among them, MWNT-g-PTMA2 containing 35.2% of PTMA showed the best performance with the initial specific capacity of 243 mAh g^{-1}. However, it showed continuous capacity fading, leading to 60% capacity retention after 250 cycles. It was found

**ADVANCED
SCIENCE NEWS**

www.advancedsciencenews.com

**ADVANCED
ENERGY &
SUSTAINABILITY
RESEARCH**
Open Access
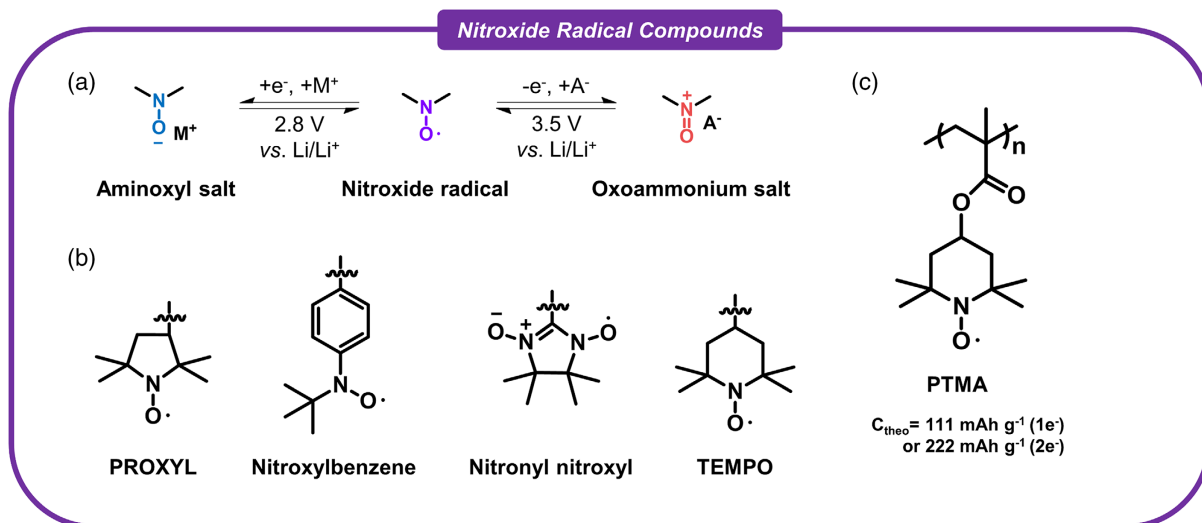
www.advenergysustres.com

Figure 16. a) The redox mechanism of the nitroxide redox center. b) The chemical structures of various nitroxide radical ROMs. c) The chemical structure of PTMA with its theoretical specific capacity.
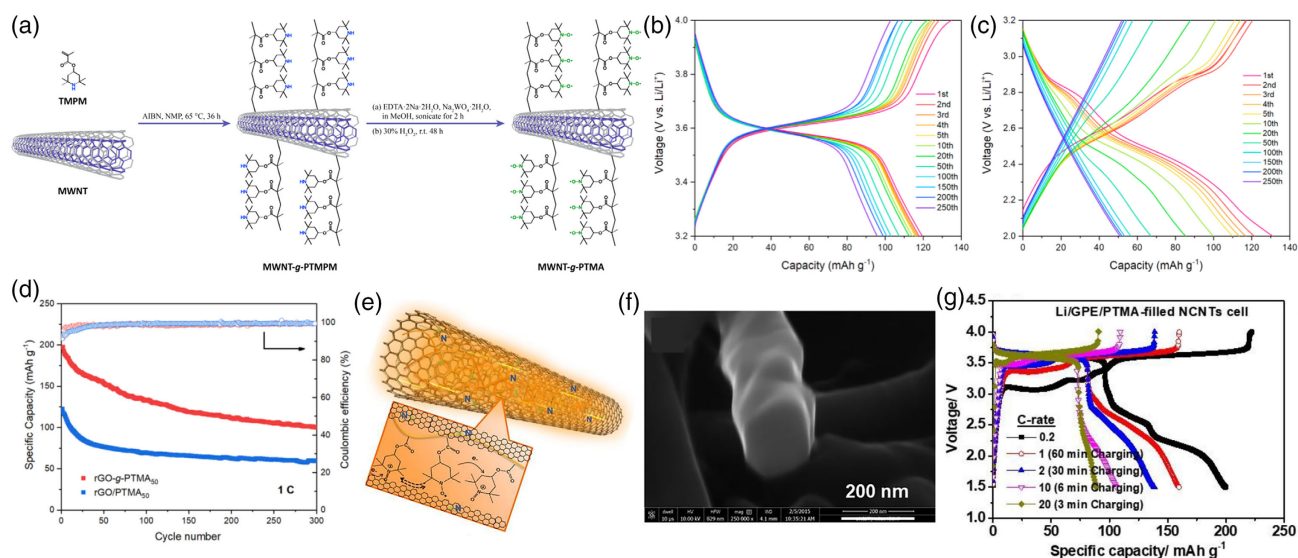

Figure 17. a) Schematic diagrams of the synthetic procedures for multiwalled carbon nanotubes (MWNT)-g-PTMA. b,c) Charge–discharge curves of the MWNT-g-PTMA composites at different voltage ranges at 1C: b) 3.2–4.0 V and c) 2.0–3.2 V versus Li/Li$^+$. Reproduced with permission.[197] Copyright 2021, Elsevier. d) The cycle stability of reduced graphene oxide (rGO)-g-PTMA$_{50}$ (chemically grafted) and rGO/PTMA$_{50}$ (physically mixed) at 1C. Reproduced with permission.[198] Copyright 2021, Elsevier. e) Schematic illustration and f) a SEM image of the PTMA-filled nitrogen-doped carbon nanotubes (NCNTs). g) The charge–discharge profiles of the PTMA-filled NCNT electrode at different current densities. Reproduced with permission.[199] Copyright 2021, Elsevier.

that the capacity fading of the composite electrode was attributed to the irreversible n-type process rather than the reversible p-type process, which was evidenced by severer capacity decay with the diminished charge/discharge voltage plateaus in the n-type voltage region (i.e., in the range of 2.0–3.2 V vs Li/Li$^+$) (Figure 17b,c).

Subsequently, using the same in situ polymerization strategy, Jin et al.[198] grafted PTMA onto the reduced graphene oxide (rGO) to fabricate rGO-g-PTMA composites with PTMA content up to 64%. The best performing rGO-g-PTMA$_{50}$ composite

(PTMA content = 50%) delivered a specific capacity of 197 mAh g^{-1} at 1C, but it also experienced severe capacity decay to 101 mAh g^{-1} after 300 cycles as similar to the MWNT-g-PTMA composites (Figure 17d). Furthermore, still low active content in the composite electrodes limited their electrode-level capacities (i.e., the specific capacity when considering the whole electrode weight) below 100 mAh g^{-1}.

Meanwhile, Byeon et al.[199] proposed a novel strategy to increase the PTMA content in the nanocarbon composites. They filled the PTMA polymers inside the pores of the

**ADVANCED
SCIENCE NEWS**

www.advancedsciencenews.com

**ADVANCED
ENERGY & SUSTAINABILITY
RESEARCH**
Open Access

www.advenergysustres.com

nitrogen-doped carbon nanotubes (NCNTs) by using the diffusion process of PTMA solution (Figure 17e,f). By repetitive filling and washing process, the PTMA content could be increased up to 72.2% in the NCNT composites. The PTMA-filled NCNT composite electrode delivered a specific capacity of 199.8 mAh g^{-1} at 0.2C with superior cycle stability over 3000 cycles (capacity retention >80%) due to suppressed dissolution of PTMA by the π–π interactions between PTMA and NCNT. However, only 45% of the capacity was retained at a high rate of 2C (Figure 17g), which was rather low-rate performance in comparison with other PTMA-based electrodes utilizing only the p-type redox.[182] The electrochemical impedance spectroscopy (EIS) studies revealed that the CT resistance and ion diffusivity of the n-type process of the PTMA-filled NCNT composite (1193.8 Ω and 1.7 $\times$ 10^{-13} cm^2 s^{-1}) were considerably lower than those of its p-type process (825.5 Ω and 6.4 $\times$ 10^{-9} cm^2 s^{-1}).

In summary, the PTMA-based electrodes showed large specific capacities ($\approx$250 mAh g^{-1}) relying on the bipolar-type redox process. However, the n-type redox ($\approx$ 2.8 V vs Li/Li$^+$) lowered their average voltage and negatively impacted on cycle stability and rate performance. What is worse, a large amount of expensive nanocarbon materials such as cabon nanotube (CNT) and graphene was essential for achieving such high performance.

3.6. Viologens

In the previous sections, we have discussed the p-type ROMs that occur in the neutral state and undergo oxidation reactions at high voltages. In contrast, viologens typically occur in the di-cationic form (V^{2+}) and undergo two single-electron reductions in a stepwise manner (**Figure 18**a): the first reduction to form a radical cation (V$^+$) and then the second reduction to form a neutral quinoid structure (V). Thus, they typically have low redox voltages (<2.5 V vs Li/Li$^+$), making them suitable for anode materials in all-organic rechargeable batteries using dual-ion or anion-shuttle mechanisms. So far, many viologen derivatives have already been studied for anolytes in the redox-flow batteries.[200,201] But, in recent years, they have attracted growing attention for the stationary-type batteries.

The first viologen-based solid-type electrode was reported by Yao and colleagues in 2015.[32] They prepared a viologen polymer poly(1,1'-pentyl-4,4'-bipyridinium dihexafluorophosphate (PBPy)) where pentyl groups linked dihexafluorophosphate viologens (Figure 18b). As shown in **Figure 19**a, the PBPy electrode showed two voltage plateaus at −0.7 and −1.2 V versus Ag$^+$/Ag (i.e., 2.6 and 2.1 V vs Li/Li$^+$) with a specific capacity of 79 mAh g^{-1} (theoretical capacity = 104 mAh g^{-1}) in the initial cycle. However, due to the low degree of polymerization, the high solubility of the polymer led to a rapid capacity drop to 36 mAh g^{-1} after 20 cycles. Nevertheless, by utilizing PBPy as an anode, they fabricated an all-organic full-cell coupled with PVK as a cathode. The full-cell delivered a specific capacity of 100 mAh g^{-1} with a voltage of 1.8 V relying on the PF$_6^-$ anion charge carrier.

To increase the voltage of full-cell, Kato et al. lowered the redox voltage of viologen ROMs by introducing an additional aromatic ring, such as phenyl, thiophene, ethylene dioxythiophene (EDOT), and pyridine, between the bipyridinium rings (Figure 18c).[33] The insertion of the additional ring effectively
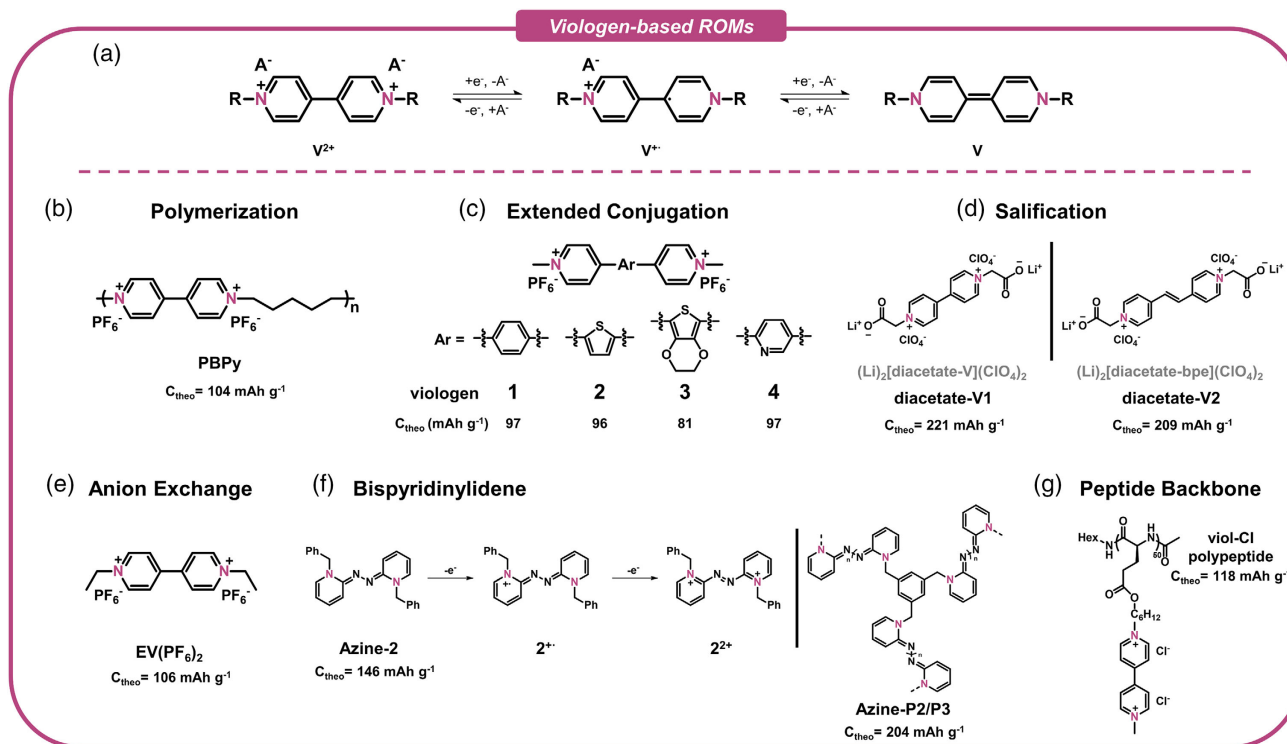

Figure 18. a) The redox mechanism of viologen. b–g) The chemical structures of the viologen derivatives reviewed in this paper.

**ADVANCED
SCIENCE NEWS**

www.advancedsciencenews.com

**ADVANCED
ENERGY & SUSTAINABILITY
RESEARCH**
Open Access
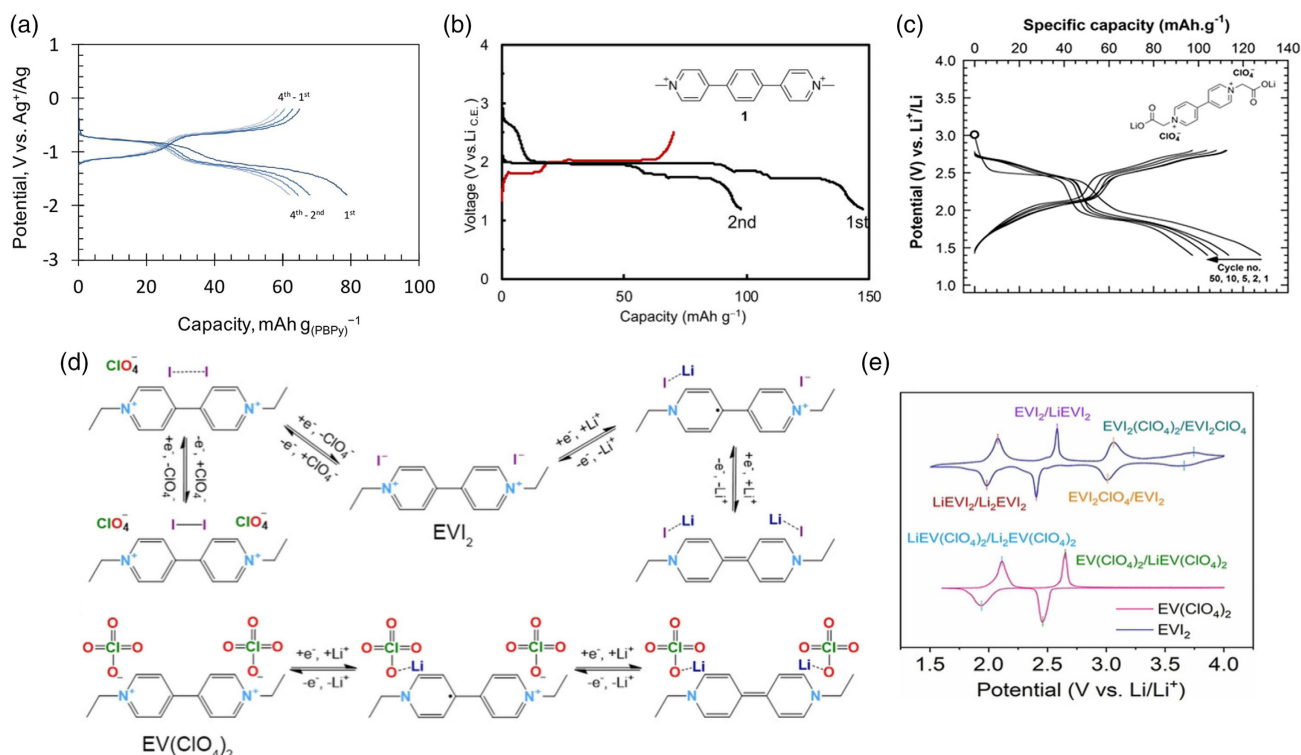
www.advenergysustres.com

Figure 19. The galvanostatic charge/discharge profiles of a) PBPy (Reproduced with permission.[33] Copyright 2015, Springer Nature), b) **viologen 1** with a phenyl as a conjugation extension linker (Reproduced with permission.[34] Copyright 2020, Wiley-VCH GmbH), and c) diacetate-V1 (Reproduced with permission.[202] Copyright 2019, Wiley-VCH GmbH). d) The proposed redox mechanisms of ethyl viologen (EVI$_2$) and redox-inactive perchlorates (EV(ClO$_4$)$_2$). e) Cyclic voltammogram of EV(ClO$_4$)$_2$ and EVI$_2$ at a scan rate of 0.2 mV s^{-1}. Reproduced with permission.[204] Copyright 2020, Wiley-VCH GmbH.

enlarged the conjugation length and spatially separated the charges, leading to lower redox voltages as predicted by DFT calculation. Furthermore, the voltage gaps between the first and the second reduction of the four viologens were also narrowed to 0.15, 0.32, 0.34, and 0.26 V for viologens (**1–4** in Figure 19b), respectively, compared to that of conventional viologens (≈0.5 V). As a result, the four viologen compounds showed lower average voltages of 1.98, 2.12, 2.07, and 2.10 V versus Li/Li$^+$ for viologen **1–4**, respectively. However, due to readily soluble nature, their cycle stability was very poor.

To suppress the dissolution, Jouhara et al. incorporated two carboxylate groups into the viologens to prepare diacetate—V1 and V2 (Figure 18d).[202] The two carboxylated viologens showed two voltage plateaus at 2.4 and 1.9 versus Li/Li$^+$ with specific capacities of 130 and 110 mAh g^{-1} for diacetate V1 and V2, respectively (Figure 19c). Their reversible reduction mechanism relying on the anion insertion/release was evidenced by ex situ Fourier-transform infrared spectroscopy (FT-IR) and ^{35}Cl magic-angle spinning (MAS)–nuclear magnetic resonance (NMR) spectroscopy. Compared to the original viologens, the cycle stability of the carboxylated ones was greatly improved. Still, progressive capacity decay was observed due to the slow dissolution during the cycle test.

Very recently, Chen et al.[203] successfully prevented the dissolution of ethyl viologen by simply exchanging the counter anions to hexafluorophosphates (Figure 18e). The ethyl viologen

(EV)(PF$_6$)$_2$ had low solubility of around 5–10 mM in 1.0 M LiClO$_4$ propylene carbonate (PC) electrolyte. Then, they prepared a viologen/carbon black composite (EV-KB) by mixing EV(PF$_6$)$_2$ with Ketjen Black (KB) in a weight ratio of 2:1 using a simple ball-milling method. Typically, many organic electrodes showed poor performance with high mass loading; however, the EV-KB composite could deliver a specific capacity of 79 mAh g^{-1} at 0.2 mA cm^{-2}, corresponding to 70% of its theoretical capacity, even with high mass loading of 9 mg cm^{-2} in the electrode.

To increase the specific capacity, Ma et al.[204] introduced redox-active iodide anions as a counter ion into the ethyl viologen (EVI$_2$) instead of the redox-inactive perchlorates (EV(ClO$_4$)$_2$) (see Figure 19d for the molecular structures). Both materials showed a typical two-step reduction of viologen in the low-voltage region (1.5–2.5 V vs Li/Li$^+$). In contrast, in the high-voltage region (2.5–4.0 V vs Li/Li$^+$), EVI$_2$ displayed two additional anodic peaks at 3.06 and 3.74 V versus Li/Li$^+$, indicating that EVI$_2$ was capable of undergoing bipolar-type redox (Figure 19e). With the aid of the additional redox, the EVI$_2$ electrode delivered a high specific capacity of 225 mAh g^{-1}, which was twice higher than that of the EV(ClO$_4$)$_2$ electrode (127 mAh g^{-1}). In addition, they proposed that the reduction process of the two viologens involved the insertion of two Li$^+$ ions rather than the releasing of two I$^-$ anions (Figure 19d). In contrast, during the oxidation process of EVI$_2$, the two I$^-$ anions were oxidized to form I$_2$. Thus, two ClO$_4^-$ anions were inserted to compensate for the positive charges

ADVANCED
SCIENCE NEWS
www.advancedsciencenews.com

ADVANCED
ENERGY & SUSTAINABILITY
RESEARCH
Open Access
www.advenergysustres.com

of the ethyl viologen molecule. The redox mechanism proposed by Ma and co-workers is opposed to the typically known mechanism of viologen so far (vide supra, Figure 18a). Therefore, more in-depth studies are highly desirable to elucidate the exact redox mechanism of the viologen-based ROMs in the batteries.

Meanwhile, bispyridinylidene materials were reported for a new p-type ROM.[205] Bispyridinylidenes are neutral organic molecules where 2-position of each two pyridines are covalently linked together by a double bond. Thus, they typically undergo two-step oxidation to form 2,2'-isomers of viologens.[206–208] Acker and co-workers introduced an azine linker between the two benzylpyridine groups to prepare Azine-2 as a model compound (Figure 18f). Azine-2 showed two reversible oxidations at 2.78 and 3.32 V versus Li/Li+, which were much higher redox voltages than typical viologens, most likely due to the introduced azine linker. To prevent the dissolution, a cross-linked polymer, Azine-P2, was prepared; still, it showed capacity fading due to hydrolysis of the hydrazone end groups in the polymer (Figure 18f). After end-capping the hydrazone groups by 2-bromo-1-methylpyridinium triflate, the polymer electrode showed stable cyclability. The end-capped Azine-P3 delivered a specific capacity of 133.4 mAh g^{-1} after the initial 10 formation cycles, and 85% of the initial capacity was retained after 200 cycles (**Figure 20**a). Furthermore, the Azine-P3 polymer electrode exhibited ultrafast rate performance with minor capacity loss even at 10C (Figure 20b).

Finally, the toxicity of the viologen-based ROMs was very recently evaluated. The highly toxic nature of viologen derivatives has already been well known.[209,210] The methyl viologen is one of the most popular herbicides, namely paraquat, banned by the European Union (EU) since 2007 due to high toxicity. To endow a battery with biodegradability and recyclability, Nguyen et al. attached dichloride viologens to a polypeptide backbone as a pendant group to prepare viol-Cl polypeptide (Figure 18g).[95] The viol-Cl electrode delivered a discharge capacity of 74.2 mAh g^{-1} at 1C with two voltage plateaus at 2.13 and 2.56 V versus Li/Li+. They tested the viability of various cells, including preosteoblast (MC3T3), mouse fibroblast (NIH/3T3), and bovine coronary venular endothelial (CVE) cells. The

viologen polypeptides exhibited toxicity toward the cells, while the degradation products of the peptides were less toxic. The demonstration of a degradable all-organic full-cell using the viologen- and TEMPO-based polypeptides showed the prospect of green and sustainable batteries.

3.7. Miscellaneous Redox Centers

In this section, various p-type ROMs relying on relatively uncommon redox centers are introduced, including coronene,[211,212] tetrathiafulvalene (TTF),[213–217] and squaraine[218] (**Figure 21**).

Coronene, a polycyclic aromatic hydrocarbon (PAH), was reported to reversibly store/release a PF$_6^-$ anion at charge and discharge voltages of 4.2 and 4.0 V versus Li/Li+, respectively.[211] The ex situ X-Ray diffraction (XRD) studies revealed that the PF$_6^-$ anions were intercalated between the (111) planes as well as the (200) planes of coronene crystals. Unfortunately, the coronene electrode delivered a low specific capacity below 40 mAh g^{-1} (**Figure 22**a), which was less than half of the theoretical capacity (89.2 mAh g^{-1}). However, it showed exceptionally high cycle stability with a capacity retention of 92% over 960 cycles.

TTF is a well-known donor molecule for highly conducting CT complexes such as TTF–TCNQ.[219,220] Typically, TTF exhibits two reversible single-electron oxidation process at 3.1 and 3.5 V versus Li/Li+, respectively, for each 1,3-dithiol-2-ylidene unit (Figure 21b). In 2012, Inatomi et al. reported bis- and tris-fused TTFs (TTP and 2,2′-bi[5-(1,3-dihthiol-2-ylidene)-1,3,4,6-tetrathiapentanylidene] (TTPY)) for p-type ROMs with high redox voltages (Figure 21c).[216] The TTPY electrode showed three oxidation peaks at 3.67, 3.89, and 4.28 V for six-electron transfer. In contrast to the low solubility in the neutral state, TTPY turned into highly soluble in the hexacationic state due to strong electrostatic repulsion between the (TTPY)$^{6+}$ molecules. Thus, they cycled the TTPY electrode below 4.05 V versus Li/Li+, limiting it to only four-electron transfer. In the voltage range of 3.00–4.05 V, the TTPY electrode delivered a specific capacity of 168 mAh g^{-1} with 84% capacity retention after 100 cycles (Figure 22b).
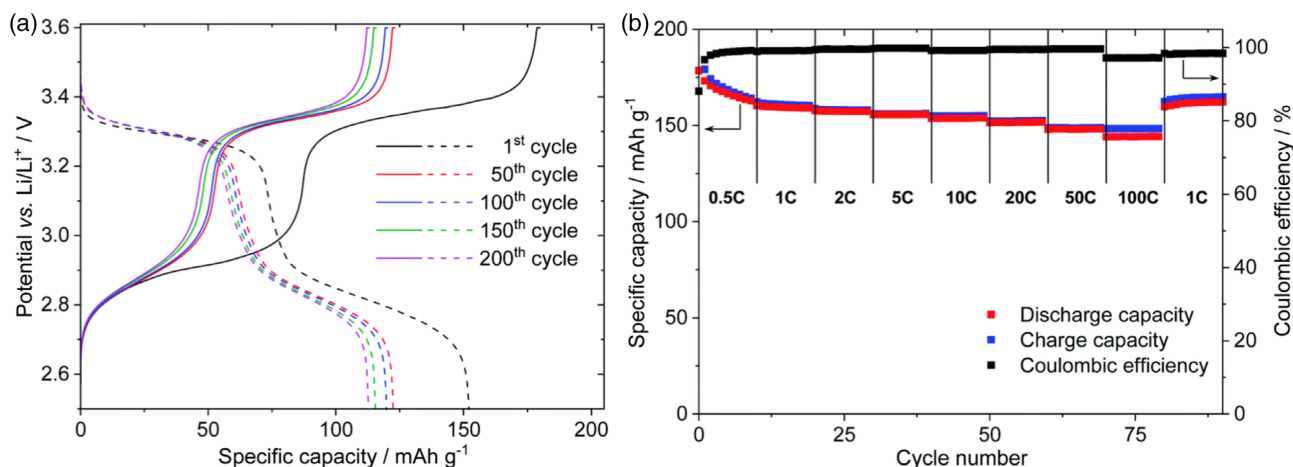

Figure 20. The electrochemical performance of the Azine-P3 electrode. a) The charge/discharge profiles at 1C for 200 cycles and b) the specific capacities at different current densities. Reproduced with permission.[205], Copyright 2020, Royal Society of Chemistry.
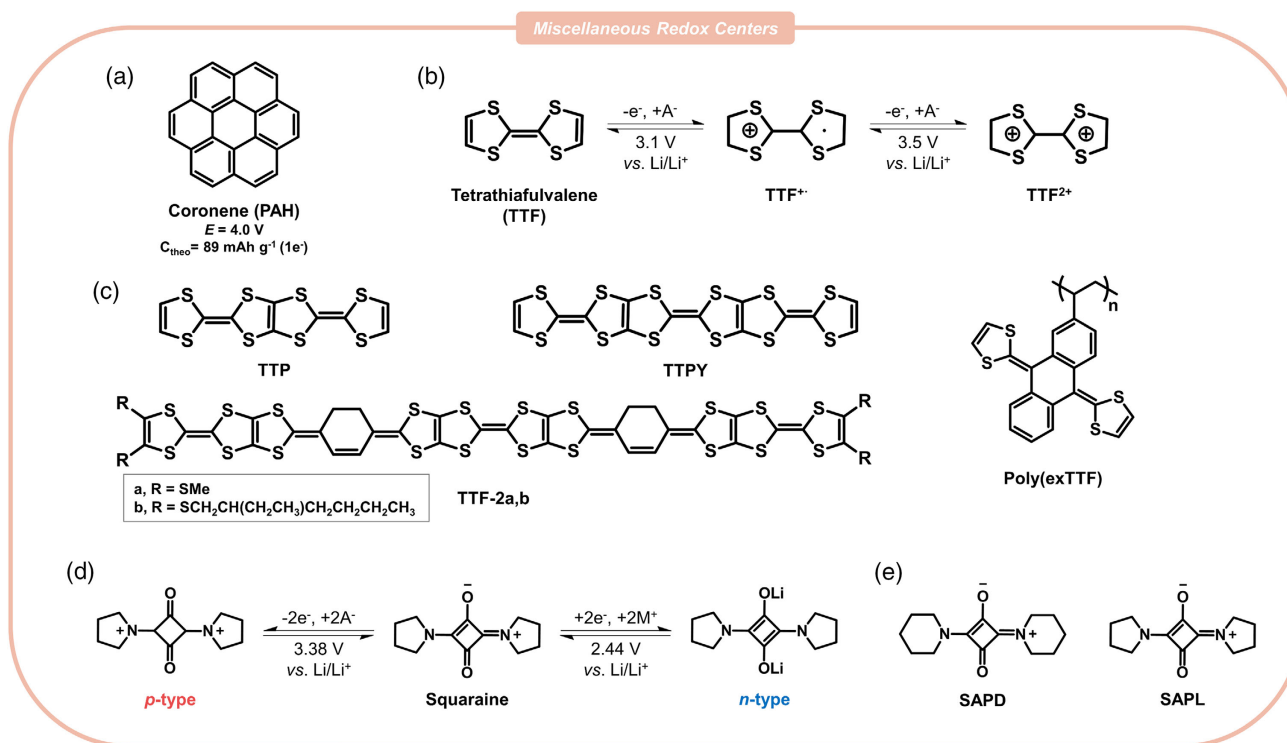
Figure 21. a–e) Molecular structures and redox mechanism of miscellaneous redox materials.

Subsequently, to suppress dissolution, Kato et al. attempted to fuse two more TTF units to prepare a pentakis-fused TTF.[217] However, the low solubility restricted the synthesis procedures. To avoid such difficulties, cyclehexnene-1,4-diylidene units were introduced as a solubilizing linker between TTF units to prepare TTF-2a (Figure 21c). The TTF-2a electrode delivered a discharge specific capacity of 196 mAh g^{-1} in the initial cycle at 0.5C, corresponding to 92% of the theoretical capacity for ten-electron transfer (Figure 22c). Due to the high average discharge voltage of 3.56 V versus Li/Li$^+$, the energy density of TTF-2a reached as high as 700 Wh kg^{-1}. Moreover, even at a high rate of 10C, it retained 64% of the low-rate specific capacity. However, the dissolution of TTF-2a in the +10 state led to poor cycle stability.

Meanwhile, Häupler et al. reported a polymer, poly(exTTF), bearing π-extended TTF units as a pendant group for an electrode material (Figure 21d).[215] In contrast to typical TTFs, the exTTF unit undergo a two-electron oxidation reaction to form a dication in a single step (Figure 22d). But due to the heavy molecular weight of the redox-inactive π-extension linker between 1,3-dithiol-2-ylidene units, the theoretical specific capacity of poly(exTTF) was limited to 132 mAh g^{-1}. At 1C, 82% of its theoretical capacity was delivered with a charge/discharge plateau of 3.5 and 3.1 V versus Li/Li$^+$. Nevertheless, it could maintain a specific capacity of 82 mAh g^{-1} even after 250 cycles.

Very recently, Zu et al. proposed squaraine derivatives for organic electrode materials with high cycle stability.[218] Squaraine consists of an electron-deficient four-membered ring between two electron-donating groups, leading to a D–A–D-type zwitterionic intramolecular CT structure (Figure 21d). Two

squaraine derivatives with different cyclic aliphatic amines were designed: 2,4-di(piperidin-1-yl)cyclobutane-1,3-dione (SAPD) with six-membered piperidinyl groups and 2,4-di(pyrrolidin-1-yl)cyclobutane-1,3-dione (SAPL) with five-membered pyrrolidinyl groups (Figure 21e). In coin-cells, the two molecules delivered high specific capacities of 284 and 371 mAh g^{-1} for SAPD and SAPL, respectively, at 0.1C in the voltage range of 0.2–3.4 V versus Li/Li$^+$ (Figure 22e). They proposed that the two squaraines underwent bipolar type redox with four-electron transfer: p-type redox for two electrons from the two tertiary amines at 3.38 V and n-type redox for two electrons from the two carbonyl groups at 2.44 V, respectively (Figure 21d). However, most of the capacity contribution seemed to originate from the n-type redox in the voltage range below 3 V versus Li/Li$^+$. It was attributed to the large polarization of p-type redox and sluggish anion kinetics, leading to a low-capacity utilization in the squaraine electrodes. Only 66% and 76% of the theoretical capacity were utilized for SAPD and SAPL, respectively. However, SAPL maintained a specific capacity of 198 mAh g^{-1} at 0.5C for 1000 cycles, corresponding to a capacity retention of 78%. The remarkable cycle stability was attributed to the alternately stacked crystal structure with the strong intermolecular dipole–dipole interactions effectively suppressing the dissolution (Figure 22f).

4. Summary and Perspectives

We have summarized the development progress of p-type ROMs, including CPs, phenylamines, dibenzo-annulated
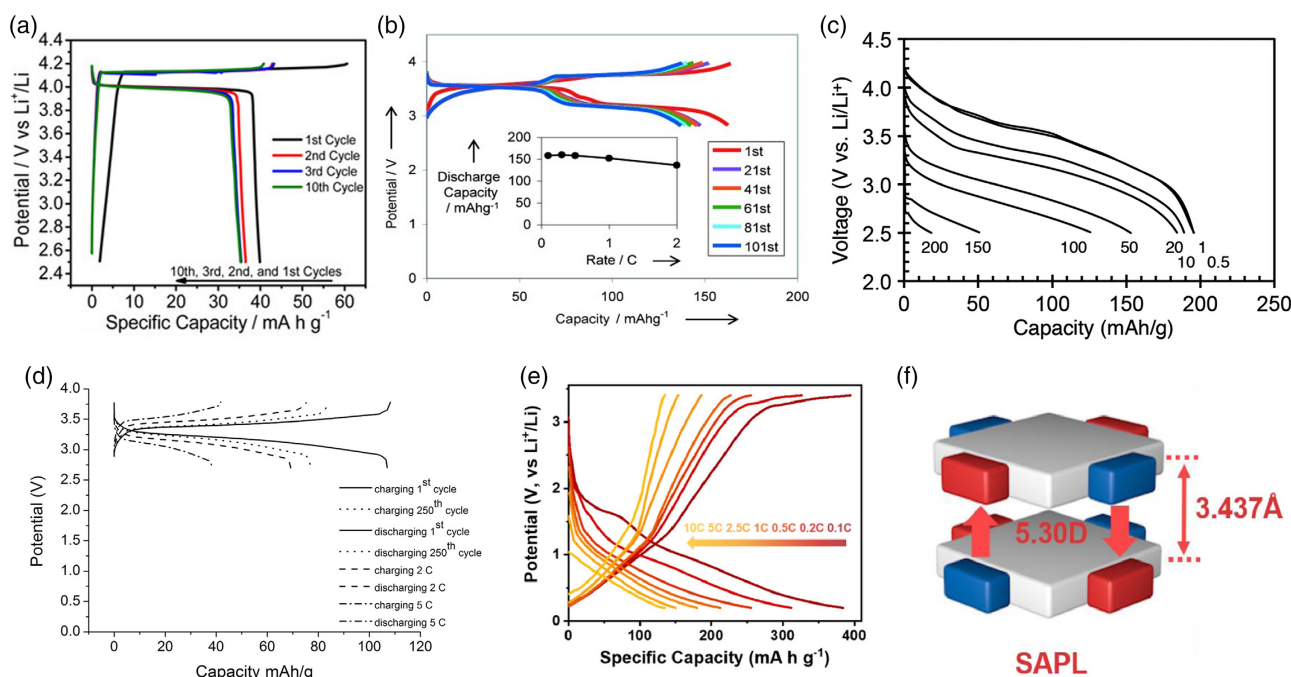
**ADVANCED
SCIENCE NEWS**

www.advancedsciencenews.com

**ADVANCED
ENERGY & SUSTAINABILITY
RESEARCH**
Open Access

www.advenergysustres.com

Figure 22. The galvanostatic charge/discharge profiles of a) the polycyclic aromatic hydrocarbon (PAH) electrode for 10 cycles at 30 mA g^{-1} (Reproduced with permission.[211] Copyright 2016, American Chemical Society) and b) the TTPY electrode over 100 cycles at 0.2C (Reproduced with permission.[216] Copyright 2012, Wiley-VCH GmbH). c) The discharge voltage curves of the tetrathiafulvalene (TTF)-2a electrode at various current densities from 0.5C to 200C. Reproduced with permission.[217] Copyright 2014, Royal Society of Chemistry. d) The charge/discharge curves of the poly(exTTF) electrode in the first and 250th cycle at 1C and in the representative cycles at different current densities. Reproduced with permission.[215] Copyright 2014, Wiley-VCH GmbH. e) The voltage–capacity profiles of the SAPL electrode at various rates from 0.1C to 1C. f) Schematic illustration of the packing structure of SAPL with the molecular dipole moments. Reproduced with permission.[218] Copyright 2021, Elsevier.

five/six-membered heterocyclic rings, nitroxide radicals, viologens, and miscellaneous compounds. In contrast to the n-type ROMs, the redox mechanism relying on the deep HOMO level provided the p-type ROMs with high working voltages above 3.0 V versus Li/Li$^+$, as shown in **Figure 23**a. It should be noted that most p-type ROMs have charge/discharge voltages comparable with conventional inorganic electrode materials such as LiCoO$_2$ (LCO) and LiFePO$_4$ (LFP) (>3.5 V vs Li/Li$^+$).[221,222] Furthermore, a dibenzo-annulated six-membered ring compound DD showed the highest voltage (≈4.2 V vs Li/Li$^+$),[91] which is even higher than that of LiMn$_2$O$_4$ (LMO) (≈4.1 V vs Li/Li$^+$).[223–235] Nevertheless, it was found that many p-type ROMs delivered low specific capacities below 150 mAh g^{-1}, which limited their specific energy lower than conventional electrode materials (<500 Wh kg^{-1}, see Figure 23a). This was attributed to the fact that most p-type ROMs relied on only a single-electron oxidation reaction. With the aid of bipolar-type double redox, the PTMA composite electrodes delivered large specific capacities (>200 mAh g^{-1}); however, the capacity contributions from the n-type reaction naturally lowered their average voltages concurrently with the specific energies.[197–199]

In contrast, the PNZ derivatives, one of the dibenzo-annulated six-membered ring compounds, undergo two stepwise single-electron oxidations, leading to large specific capacities of ≈230 mAh g^{-1} with specific energies higher than 600 Wh kg^{-1}.[65,155–158] Impressively, the PNZ network polymer

poly(Ph-PZ)-10 delivered the highest specific energy (≈800 Wh kg^{-1}) among p-type ROMs, which far exceeds that of conventional electrodes.[157] The TTF compounds also delivered large specific capacities (≈200 mAh g^{-1}) with moderately high voltages.[214,216,217] A promisingly high specific energy of ≈760 Wh kg^{-1} was also demonstrated by the PXZ compound Et-PXZ; however, the electrolyte optimization to utilize the second redox inevitably lowered its average working voltage.[161] Meanwhile, in the low voltage range (<2.5 V vs Li/Li$^+$), the viologen derivatives are the only choice for anode materials in all-organic full-cells using the anion-redox shuttle mechanism.[32,33,95,202,203] Therefore, for more practical use, designing new *p*-type ROMs possessing a further low redox voltage (<2.0 V vs Li/Li$^+$) with a larger specific capacity (>200 mAh g^{-1}) is highly desired.

From the viewpoint of cycle stability, small-molecule p-type ROMs are inferior to polymeric materials due to the dissolution in the electrolytes (Figure 23b). For stable cycling, some small molecules often required fabrication of composites with nanocarbons, such as CNT[161] and ordered mesoporous carbon (commercial named CMK3),[170] or CT complexes with n-type ROMs.[91] What is worse, in most reports, they were evaluated for relatively short cycles (e.g., 100–1000 cycles). In contrast, linear polymerization or constructing network structures (e.g., cross-linked polymers, COFs, etc.) effectively improved the cycle stability of p-type ROMs. As displayed in
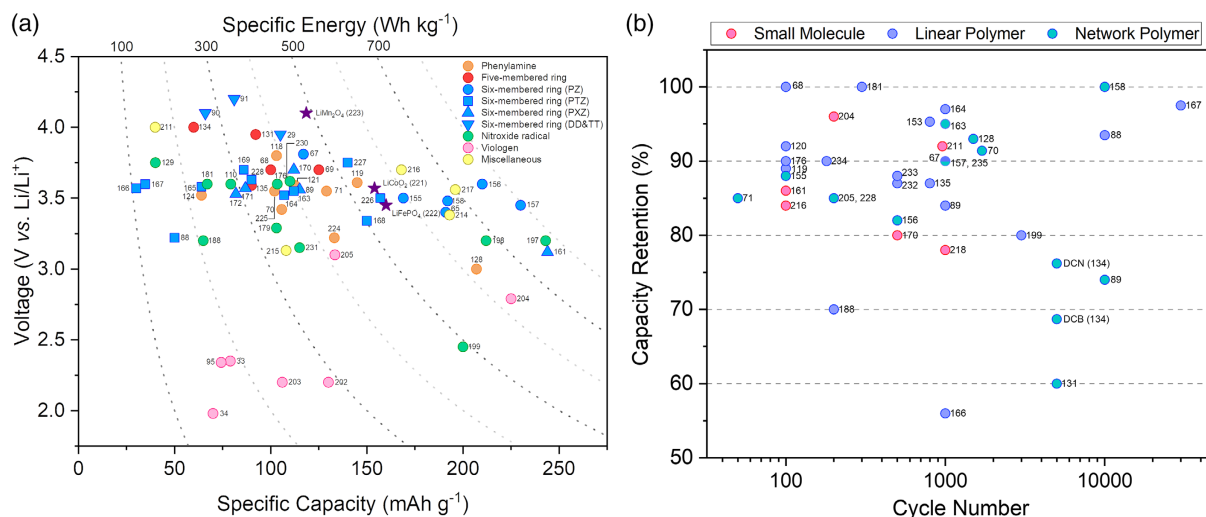
Figure 23. Summaries of the electrochemical performance of reported p-type ROMs. a) A voltage versus specific capacity plot with specific energy depending on the redox center categories. b) A capacity retention versus cycle number plot according to the types of ROMs. The numbers in the figure correspond to the number of references in this paper. The detailed data are summarized in Table S1 and S2, Supporting Information.

Figure 23b, most polymeric p-type ROMs (i.e., both linear and network polymers) exhibited outstanding capacity retention (>85%) except the Cbz-based ROMs cross-linked by the in situ electrochemical method.[131,134] Most impressively, an exceptionally stable cyclability was shown by a PNZ-based network polymer TzPz, which retained 99% of the initial capacity even after 10 000 cycles.[158] In contrast, several PTZ polymers also showed high cycle stability over ultra-long cycles (>1000–10 000 cycles); but they mostly delivered low specific capacities below 50 mAh g^{-1}.[88,167]

Since the demands for EVs and energy storage system (ESSs) are rapidly growing, the rate capability has become a crucial factor for batteries. As shown in **Figure 24**, it is worth noting that the p-type ROMs typically exhibited remarkable specific powers allowing rapid charge/discharge (<5 min), attributed most likely to the fast diffusion kinetics of anions and the flexible nature of intermolecular packing structures. To our surprise, two PNZ-based polymers[156,157] could deliver specific energies of more than 600 Wh kg^{-1} within a time even shorter than 1 min (i.e., specific powers >40 000 W kg^{-1}), which is a markedly superior rate capability than LCO and LFP. Among the small molecules, the TTF-2a electrode exhibited an excellent rate capability.[217]

In conclusion, the p-type ROMs showed promising performances, so far, at the material level in terms of redox voltage, specific energy, cycle stability, and specific power. However, it should also be noted that such performances were mostly achieved from thin electrodes with small areas and rather low active content (≈60 wt%) in coin-type half-cells due to low electrical conductivity. To increase the electrical conductivity of ROMs, various strategies have been reported to date, for example, i) introducing carbon nanomaterials, such as CNT,[119] graphene,[198] and CMK3[170]; ii) incorporation of π-conjugated backbones[117,167,188]; and iii) formation of the CT complexes with donor–acceptor materials.[91,219] However, such strategies further require expensive nanocarbons or complicated synthesis procedures, while the overall performance at the electrode- and
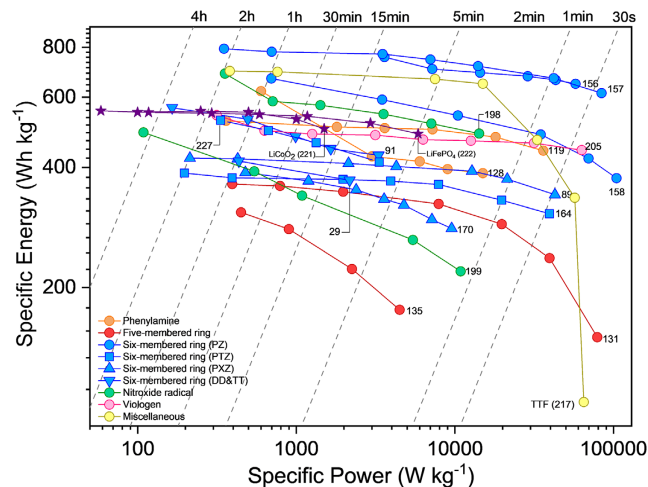

Figure 24. A Ragone plot with a comparison of the p-type ROMs and conventional inorganic materials. The numbers in the figure correspond to the number of references in this paper. The detailed data are summarized in Table S1 and S2, Supporting Information.

cell-level was not much improved. Therefore, further research should focus on improving the electrochemical performance of p-type ROMs at the electrode and the full-cell level.

To this end, modifying the molecular designs of the existing ROMs, developing facile electrode fabrication processes, and optimizing the electrolyte composition are highly desired. In particular, despite the high working voltage of the p-type ROMs, further application is hindered due to lack of stable electrolytes at the high voltages. Several pioneering studies to develop high-voltage electrolytes for LIBs have recently been published[236,237]; therefore, efforts to apply them to the p-type ROMs are highly desired. In addition, for achieving high cycle stability, use of ionic liquids (ILs) and solid-state electrolytes would be a good option to prevent dissolution of p-type ROMs.[238–241] But,

research using such electrolytes for the organic electrode materials is still in infancy.

In addition, since the p-type ROMs rely on anion chemistry, they are not suitable for typical metal-ion batteries. Thus, to diversify the anode candidates for all-organic full-cells, identifying new p-type redox centers possessing low redox voltages and improving the performance of viologen-based ROMs are also imperative.

Above all, it is obvious that a fundamental understanding of the exact redox mechanism and the anion chemistry not only at the molecular level but also at the intermolecular level is a prerequisite. In this context, in situ or operando analyses of p-type ROMs are highly desired to monitor their changes in the chemical composition, morphology, nano- (or micro-) structures, and crystallinity during charge/discharge. Recently, a few studies to elucidate the redox mechanism of ROMs have been reported using in situ (or operando) FT-IR, FT-Raman, and XRD.[204,242,243] But, more advanced techniques such as in situ (or operando) X-Ray photoelectron spectroscopy (XPS), SEM, and transmission electron microscope (TEM) will be needed to get further insight into the redox mechanism of p-type ROMs.

Supporting Information

Supporting Information is available from the Wiley Online Library or from the author.

Acknowledgements

Conflict of Interest

The authors declare no conflict of interest.

Keywords

[1] V. Etacheri, R. Marom, R. Elazari, G. Salitra, D. Aurbach, *Energy Environ. Sci.* **2011**, *4*, 3243.
[2] F. Sun, M. Osenberg, K. Dong, D. Zhou, A. Hilger, C. J. Jafta, S. Risse, Y. Lu, H. Markötter, I. Manke, *ACS Energy Lett.* **2018**, *3*, 356.
[3] C.-C. Li, Y.-W. Wang, *J. Power Sources* **2013**, *227*, 204.
[4] Z. Gong, Y. Yang, *Energy Environ. Sci.* **2011**, *4*, 3223.
[5] B. C. Melot, J.-M. Tarascon, *Acc. Chem. Res.* **2013**, *46*, 1226.
[6] J. B. Goodenough, Y. Kim, *Chem. Mater.* **2010**, *22*, 587.
[7] M. S. Whittingham, *Chem. Rev.* **2004**, *104*, 4271.
[8] K. Turcheniuk, D. Bondarev, V. Singhal, G. Yushin, *Nature* **2018**, *559*, 467.
[9] T. Perveen, M. Siddiq, N. Shahzad, R. Ihsan, A. Ahmad, M. I. Shahzad, *Renewable Sustainable Energy Rev.* **2020**, *119*, 109549.
[10] X. Pu, H. Wang, D. Zhao, H. Yang, X. Ai, S. Cao, Z. Chen, Y. Cao, *Small* **2019**, *15*, 1805427.
[11] X. Min, J. Xiao, M. Fang, W. A. Wang, Y. Zhao, Y. Liu, A. M. Abdelkader, K. Xi, R. V. Kumar, Z. Huang, *Energy Environ. Sci.* **2021**, *14*, 2186.
[12] W. Zhang, Y. Liu, Z. Guo, *Sci. Adv.* **2019**, *5*, eaav7412.
[13] X.-X. Luo, W.-H. Li, H.-J. Liang, H.-X. Zhang, K.-D. Du, X.-T. Wang, X.-F. Liu, J.-P. Zhang, X.-L. Wu, *Angew. Chem., Int. Ed.* **2022**, *61*, 202117661.
[14] G.-P. Yang, X.-X. Luo, Y.-F. Liu, K. Li, X.-L. Wu, *ACS Appl. Mater. Interfaces* **2021**, *13*, 46902.
[15] M.-C. Lin, M. Gong, B. Lu, Y. Wu, D.-Y. Wang, M. Guan, M. Angell, C. Chen, J. Yang, B.-J. Hwang, *Nature* **2015**, *520*, 324.
[16] C. You, X. Wu, X. Yuan, Y. Chen, L. Liu, Y. Zhu, L. Fu, Y. Wu, Y.-G. Guo, T. van Ree, *J. Mater. Chem. A* **2020**, *8*, 25601.
[17] C. Xu, B. Li, H. Du, F. Kang, *Angew. Chem.* **2012**, *124*, 957.
[18] M. Song, H. Tan, D. Chao, H. J. Fan, *Adv. Funct. Mater.* **2018**, *28*, 1802564.
[19] J. Xie, Q. Zhang, *Small* **2019**, *15*, 1805061.
[20] C. N. Gannett, L. Melecio-Zambrano, M. J. Theibault, B. M. Peterson, B. P. Fors, H. D. Abruña, *Mater. Rep.: Energy* **2021**, *1*, 100008.
[21] P. Poizot, J. Gaubicher, S. Renault, L. Dubois, Y. Liang, Y. Yao, *Chem. Rev.* **2020**, *120*, 6490.
[22] S. Muench, A. Wild, C. Friebe, B. Häupler, T. Janoschka, U. S. Schubert, *Chem. Rev.* **2016**, *116*, 9438.
[23] Y. Lu, J. Chen, *Nat. Rev. Chem.* **2020**, *4*, 127.
[24] Y. Liang, Y. Yao, *Joule* **2018**, *2*, 1690.
[25] D. J. Min, K. Lee, S. Y. Park, J. E. Kwon, *ChemSusChem* **2020**, *13*, 2303.
[26] D. J. Min, F. Miomandre, P. Audebert, J. E. Kwon, S. Y. Park, *ChemSusChem* **2019**, *12*, 503.
[27] S. Lee, J. E. Kwon, J. Hong, S. Y. Park, K. Kang, *J. Mater. Chem. A* **2019**, *7*, 11438.
[28] A. Wild, M. Strumpf, B. Häupler, M. D. Hager, U. S. Schubert, *Adv. Energy Mater* **2017**, *7*, 1601415.
[29] T. Suga, H. Ohshiro, S. Sugita, K. Oyaizu, H. Nishide, *Adv. Mater.* **2009**, *21*, 1627.
[30] N. Casado, D. Mantione, D. Shanmukaraj, D. Mecerreyes, *ChemSusChem* **2020**, *13*, 2464.
[31] L. Zhu, A. Lei, Y. Cao, X. Ai, H. Yang, *Chem. Commun.* **2013**, *49*, 567.
[32] M. Yao, H. Sano, H. Ando, T. Kiyobayashi, *Sci. Rep.* **2015**, *5*, 1.
[33] M. Kato, H. Sano, T. Kiyobayashi, M. Yao, *ChemSusChem* **2020**, *13*, 2379.
[34] K. Hatakeyama-Sato, T. Tezuka, R. Ichinoi, S. Matsumono, K. Sadakuni, K. Oyaizu, *ChemSusChem* **2020**, *13*, 2443.
[35] E. Deunf, P. Moreau, E. Quarez, D. Guyomard, F. Dolhem, P. Poizot, *J. Mater. Chem. A* **2016**, *4*, 6131.
[36] V. Cadiou, A. C. Gaillot, É. Deunf, F. Dolhem, L. Dubois, T. Gutel, P. Poizot, *ChemSusChem* **2020**, *13*, 2345.
[37] P. Poizot, F. Dolhem, *Energy Environ. Sci.* **2011**, *4*, 2003.
[38] D. Larcher, J.-M. Tarascon, *Nat. Chem.* **2015**, *7*, 19.
[39] K. Deuchert, S. Hünig, *Angew. Chem., Int. Ed. Engl.* **1978**, *17*, 875.
[40] B. Esser, *Org. Mater.* **2019**, *1*, 063.
[41] B. Esser, F. Dolhem, M. Becuwe, P. Poizot, A. Vlad, D. Brandell, *J. Power Sources* **2021**, *482*, 228814.
[42] J. Kaufman, T. C. Chung, A. Heeger, F. Wudl, *J. Electrochem. Soc.* **1984**, *131*, 2092.
[43] F. Goto, K. Abe, K. Ikabayashi, T. Yoshida, H. Morimoto, *J. Power Sources* **1987**, *20*, 243.
[44] S. Taguchi, T. Tanaka, *J. Power Sources* **1987**, *20*, 249.

[45] L. W. Shacklette, R. L. Elsenbaumer, R. R. Chance, J. M. Sowa, D. M. Ivory, G. G. Miller, R. H. Baughman, *J. Chem. Soc. Chem. Commun.* **1982**, 361.

[46] K. Nakahara, S. Iwasa, M. Satoh, Y. Morioka, J. Iriyama, M. Suguro, E. Hasegawa, *Chem. Phys. Lett.* **2002**, *359*, 351.

[47] H. Nishide, S. Iwasa, Y.-J. Pu, T. Suga, K. Nakahara, M. Satoh, *Electrochim. Acta* **2004**, *50*, 827.

[48] K. Nakahara, K. Oyaizu, H. Nishide, *Chem. Lett.* **2011**, *40*, 222.

[49] K. Nakahara, J. Iriyama, S. Iwasa, M. Suguro, M. Satoh, E. J. Cairns, *J. Power Sources* **2007**, *165*, 870.

[50] T. Suga, Y.-J. Pu, S. Kasatori, H. Nishide, *Macromolecules* **2007**, *40*, 3167.

[51] T. Suga, H. Konishi, H. Nishide, *Chem. Commun.* **2007**, 1730.

[52] Z. Song, Y. Qian, M. L. Gordin, D. Tang, T. Xu, M. Otani, H. Zhan, H. Zhou, D. Wang, *Angew. Chem.* **2015**, *127*, 14153.

[53] K. Zhang, C. Guo, Q. Zhao, Z. Niu, J. Chen, *Adv. Sci* **2015**, *2*, 1500018.

[54] J. E. Kwon, C.-S. Hyun, Y. J. Ryu, J. Lee, D. J. Min, M. J. Park, B.-K. An, S. Y. Park, *J. Mater. Chem. A* **2018**, *6*, 3134.

[55] W. Huang, Z. Zhu, L. Wang, S. Wang, H. Li, Z. Tao, J. Shi, L. Guan, J. Chen, *Angew. Chem., Int. Ed.* **2013**, *52*, 9162.

[56] H. Yang, J. Lee, J. Y. Cheong, Y. Wang, G. Duan, H. Hou, S. Jiang, I.-D. Kim, *Energy Environ. Sci.* **2021**, *14*, 4228.

[57] C. Han, H. Li, R. Shi, T. Zhang, J. Tong, J. Li, B. Li, *J. Mater. Chem. A* **2019**, *7*, 23378.

[58] M. R. Biradar, S. V. Bhosale, P. P. Morajakar, S. V. Bhosale, *Fuel* **2022**, *310*, 122487.

[59] J. Wu, X. Rui, C. Wang, W.-B. Pei, R. Lau, Q. Yan, Q. Zhang, *Adv. Energy Mater.* **2015**, *5*, 1402189.

[60] H. Senoh, M. Yao, H. Sakaebe, K. Yasuda, Z. Siroma, *Electrochim. Acta* **2011**, *56*, 10145.

[61] Y. Liang, P. Zhang, S. Yang, Z. Tao, J. Chen, *Adv. Energy Mater* **2013**, *3*, 600.

[62] Q. Zhao, J. Wang, C. Chen, T. Ma, J. Chen, *Nano Res.* **2017**, *10*, 4245.

[63] M. Armand, S. Grugeon, H. Vezin, S. Laruelle, P. Ribière, P. Poizot, J.-M. Tarascon, *Nat. Mater* **2009**, *8*, 120.

[64] Y. Shi, H. Tang, S. Jiang, L. V. Kayser, M. Li, F. Liu, F. Ji, D. J. Lipomi, S. P. Ong, Z. Chen, *Chem. Mater.* **2018**, *30*, 3508.

[65] M. Lee, J. Hong, B. Lee, K. Ku, S. Lee, C. B. Park, K. Kang, *Green Chem.* **2017**, *19*, 2980.

[66] G. Dai, X. Wang, Y. Qian, Z. Niu, X. Zhu, J. Ye, Y. Zhao, X. Zhang, *Energy Storage Mater.* **2019**, *16*, 236.

[67] F. Zhang, Y. Cheng, Z. Niu, J. Ye, G. Dai, X. Zhang, Y. Zhao, *ChemElectroChem* **2020**, *7*, 1781.

[68] J. Kim, H.-S. Park, T.-H. Kim, S. Y. Kim, H.-K. Song, *Phys. Chem. Chem. Phys.* **2014**, *16*, 5295.

[69] M. Yao, H. Senoh, T. Sakai, T. Kiyobayashi, *J. Power Sources* **2012**, *202*, 364.

[70] C. Zhang, X. Yang, W. Ren, Y. Wang, F. Su, J.-X. Jiang, *J. Power Sources* **2016**, *317*, 49.

[71] C. Su, F. Yang, L. Ji, L. Xu, C. Zhang, *J. Mater. Chem. A* **2014**, *2*, 20083.

[72] K. Hayamizu, *Electrochim. Acta* **2017**, *254*, 101.

[73] J. Huang, X. Dong, Z. Guo, Y. Wang, *Angew. Chem., Int. Ed.* **2020**, *59*, 18322.

[74] C. Han, J. Zhu, C. Zhi, H. Li, *J. Mater. Chem. A* **2020**, *8*, 15479.

[75] V. Singh, S. Kim, J. Kang, H. R. Byon, *Nano Res.* **2019**, *12*, 1988.

[76] E. Sánchez-Díez, E. Ventosa, M. Guarnieri, A. Trovò, C. Flox, R. Marcilla, F. Soavi, P. Mazur, E. Aranzabe, R. Ferret, *J. Power Sources* **2021**, *481*, 228804.

[77] Y. Y. Lai, X. Li, Y. Zhu, *ACS Appl. Polym. Mater.* **2020**, *2*, 113.

[78] P. Leung, A. Shah, L. Sanz, C. Flox, J. Morante, Q. Xu, M. Mohamed, C. P. De León, F. Walsh, *J. Power Sources* **2017**, *360*, 243.

[79] J. Luo, B. Hu, M. Hu, Y. Zhao, T. L. Liu, *ACS Energy Lett.* **2019**, *4*, 2220.

[80] D. J. Min, K. Lee, H. Park, J. E. Kwon, S. Y. Park, *Molecules* **2021**, *26*, 894.

[81] H. Kim, J. E. Kwon, B. Lee, J. Hong, M. Lee, S. Y. Park, K. Kang, *Chem. Mater.* **2015**, *27*, 7258.

[82] Z. Song, H. Zhan, Y. Zhou, *Angew. Chem., Int. Ed.* **2010**, *49*, 8444.

[83] A. Lakraychi, E. Deunf, K. Fahsi, P. Jimenez, J.-P. Bonnet, F. Djedaini-Pilard, M. Bécuwe, P. Poizot, F. Dolhem, *J. Mater. Chem. A* **2018**, *6*, 19182.

[84] S. Renault, S. Gottis, A.-L. Barrès, M. Courty, O. Chauvet, F. Dolhem, P. Poizot, *Energy Environ. Sci.* **2013**, *6*, 2124.

[85] J. Wang, A. E. Lakraychi, X. Liu, L. Sieuw, C. Morari, P. Poizot, A. Vlad, *Nat. Mater* **2021**, *20*, 665.

[86] L. Sieuw, A. E. Lakraychi, D. Rambabu, K. Robeyns, A. Jouhara, G. Borodi, C. Morari, P. Poizot, A. Vlad, *Chem. Mater.* **2020**, *32*, 9996.

[87] A. Jouhara, N. Dupré, A.-C. Gaillot, D. Guyomard, F. Dolhem, P. Poizot, *Nat. Commun.* **2018**, *9*, 1.

[88] M. Kolek, F. Otteny, P. Schmidt, C. Mück-Lichtenfeld, C. Einholz, J. Becking, E. Schleicher, M. Winter, P. Bieker, B. Esser, *Energy Environ. Sci.* **2017**, *10*, 2334.

[89] F. Otteny, V. Perner, D. Wassy, M. Kolek, P. Bieker, M. Winter, B. Esser, *ACS Sustainable Chem. Eng.* **2019**, *8*, 238.

[90] M. E. Speer, M. Kolek, J. J. Jassoy, J. Heine, M. Winter, P. M. Bieker, B. Esser, *Chem. Commun.* **2015**, *51*, 15261.

[91] S. Lee, J. Hong, S.-K. Jung, K. Ku, G. Kwon, W. M. Seong, H. Kim, G. Yoon, I. Kang, K. Hong, *Energy Storage Mater.* **2019**, *20*, 462.

[92] L. Zhang, H. Wang, X. Zhang, Y. Tang, *Adv. Funct. Mater.* **2021**, *31*, 2010958.

[93] Q. Liu, Y. Wang, X. Yang, D. Zhou, X. Wang, P. Jaumaux, F. Kang, B. Li, X. Ji, G. Wang, *Chem* **2021**, *7*, 1993.

[94] Q. Dou, N. Wu, H. Yuan, K. H. Shin, Y. Tang, D. Mitlin, H. S. Park, *Chem. Soc. Rev* **2021**, *50*, 6734.

[95] T. P. Nguyen, A. D. Easley, N. Kang, S. Khan, S.-M. Lim, Y. H. Rezenom, S. Wang, D. K. Tran, J. Fan, R. A. Letteri, *Nature* **2021**, *593*, 61.

[96] W.-H. Li, Y.-M. Li, X.-F. Liu, Z.-Y. Gu, H.-J. Liang, X.-X. Zhao, J.-Z. Guo, X.-L. Wu, *Adv. Funct. Mater.* **2022**, 2201038.

[97] W.-H. Li, H.-J. Liang, X.-K. Hou, Z.-Y. Gu, X.-X. Zhao, J.-Z. Guo, X. Yang, X.-L. Wu, *J. Energy Chem.* **2020**, *50*, 416.

[98] K. D. Fong, J. Self, K. M. Diederichsen, B. M. Wood, B. D. McCloskey, K. A. Persson, *ACS Cent. Sci.* **2019**, *5*, 1250.

[99] K. Hayamizu, *J. Chem. Eng. Data* **2012**, *57*, 2012.

[100] J. Zhao, L. Wang, X. He, C. Wan, C. Jiang, *J. Electrochem. Soc.* **2008**, *155*, A292.

[101] H. Nishide, K. Koshika, K. Oyaizu, *Pure Appl. Chem.* **2009**, *81*, 1961.

[102] R. R. Kapaev, I. S. Zhidkov, E. Z. Kurmaev, K. J. Stevenson, P. A. Troshin, *J. Mater. Chem. A* **2019**, *7*, 22596.

[103] X. Liu, Z. Ye, *Adv. Energy Mater.* **2021**, *11*, 2003281.

[104] Y. Hu, Y. Gao, L. Fan, Y. Zhang, B. Wang, Z. Qin, J. Zhou, B. Lu, *Adv. Energy Mater.* **2020**, *10*, 2002780.

[105] E. Deunf, P. Jiménez, D. Guyomard, F. Dolhem, P. Poizot, *Electrochem. Commun.* **2016**, *72*, 64.

[106] H. Shirakawa, E. J. Louis, A. G. MacDiarmid, C. K. Chiang, A. J. Heeger, *J. Chem. Soc. Chem. Commun.* **1977**, 578.

[107] J.-Z. Wang, S.-L. Chou, H. Liu, G. X. Wang, C. Zhong, S. Y. Chew, H. K. Liu, *Mater. Lett.* **2009**, *63*, 2352.

[108] J. Desilvestro, W. Scheifele, O. Haas, *J. Electrochem. Soc.* **1992**, *139*, 2727.

[109] A. Kitani, M. Kaya, K. Sasaki, *J. Electrochem. Soc.* **1986**, *133*, 1069.

[110] M. Aydın, B. Esat, Ç. Kılıç, M. Köse, A. Ata, F. Yılmaz, *Eur. Polym. J.* **2011**, *47*, 2283.

[111] Z. Cai, G. Yang, *Synth. Met.* **2010**, *160*, 1902.

[112] T. A. Skotheim, *Handbook of Conducting Polymers*, CRC Press, Boca Raton, FL **1997**.

[113] J. Xie, P. Gu, Q. Zhang, *ACS Energy Lett.* **2017**, *2*, 1985.

[114] T. Janoschka, M. D. Hager, U. S. Schubert, *Adv. Mater.* **2012**, *24*, 6397.

[115] P. Novák, K. Müller, K. Santhanam, O. Haas, *Chem. Rev.* **1997**, *97*, 207.

[116] X. Jia, Y. Ge, L. Shao, C. Wang, G. G. Wallace, *ACS Sustainable Chem. Eng.* **2019**, *7*, 14321.

[117] Y. Liang, Z. Chen, Y. Jing, Y. Rong, A. Facchetti, Y. Yao, *J. Am. Chem. Soc.* **2015**, *137*, 4956.

[118] J. Feng, Y. Cao, X. Ai, H. Yang, *J. Power Sources* **2008**, *177*, 199.

[119] F. A. Obrezkov, A. F. Shestakov, S. G. Vasil'ev, K. J. Stevenson, P. A. Troshin, *J. Mater. Chem. A* **2021**, *9*, 2864.

[120] T.-T. Truong, G. W. Coates, H. D. Abruña, *Chem. Commun.* **2015**, *51*, 14674.

[121] F. A. Obrezkov, E. S. Fedina, A. I. Somova, A. V. Akkuratov, K. J. Stevenson, *ACS Appl. Energy Mater.* **2021**, *4*, 11827.

[122] K. Yamamoto, D. Suemasa, K. Masuda, K. Aita, T. Endo, *ACS Appl. Mater. Interfaces* **2018**, *10*, 6346.

[123] C. Su, F. Yang, Y. Ye, L. Xu, L. Wang, C. Zhang, *J. Electrochem. Soc.* **2013**, *160*, A2021.

[124] C.-J. Yao, Z. Wu, J. Xie, F. Yu, W. Guo, Z. J. Xu, D.-S. Li, S. Zhang, Q. Zhang, *ChemSusChem* **2020**, *13*, 2457.

[125] T. Sun, J. Xie, W. Guo, D.-S. Li, Q. Zhang, *Adv. Energy Mater.* **2020**, *10*, 1904199.

[126] L. Yu, X. Zhou, L. Lu, X. Wu, F. Wang, *ChemSusChem* **2020**, *13*, 5361.

[127] Y. Tao, W. Ji, X. Ding, B.-H. Han, *J. Mater. Chem. A* **2021**, *9*, 7336.

[128] M. Wu, Y. Zhao, R. Zhao, J. Zhu, J. Liu, Y. Zhang, C. Li, Y. Ma, H. Zhang, Y. Chen, *Adv. Funct. Mater.* **2021**, *32*, 2107703.

[129] Y. Shirota, T. Nogami, N. Noma, T. Kakuta, H. Saito, *Synth. Met.* **1991**, *41*, 1169.

[130] Y. Lu, Q. Zhang, L. Li, Z. Niu, J. Chen, *Chem* **2018**, *4*, 2786.

[131] C. Zhao, Z. Chen, W. Wang, P. Xiong, B. Li, M. Li, J. Yang, Y. Xu, *Angew. Chem., Int. Ed.* **2020**, *59*, 11992.

[132] B. R. Hsieh, M. H. Litt, *Macromolecules* **1986**, *19*, 521.

[133] J. F. Ambrose, L. L. Carpenter, R. F. Nelson, *J. Electrochem. Soc.* **1975**, *122*, 876.

[134] Z. Wang, J. Yang, Z. Chen, L. Ye, Y. Xu, *ChemSusChem* **2021**, *14*, 4573.

[135] G. Dai, Y. Gao, Z. Niu, P. He, X. Zhang, Y. Zhao, H. Zhou, *ChemSusChem* **2020**, *13*, 2264.

[136] P. J. Jesuraj, S. Somasundaram, E. Kamaraj, H. Hafeez, C. Lee, D. Kim, S. H. Won, S. T. Shin, M. Song, C.-S. Kim, *Org. Electron.* **2020**, *85*, 105825.

[137] R. Grisorio, B. Roose, S. Colella, A. Listorti, G. P. Suranna, A. Abate, *ACS Energy Lett.* **2017**, *2*, 1029.

[138] Z. Zheng, Q. Dong, Q. Gou, J.-H. Su, J. Huang, *J. Mater. Chem. C* **2014**, *2*, 9858.

[139] M. Almtiri, T. J. Dowell, I. Chu, D. O. Wipf, C. N. Scott, *ACS Appl. Polym. Mater.* **2021**, *3*, 2988.

[140] Y. C. Choi, R. S. Kumar, N. Mergu, J. Jeong, Y.-A. Son, *Synth. Met.* **2018**, *240*, 1.

[141] U. Balijapalli, Y. T. Lee, B. S. Karunathilaka, G. Tumen-Ulzii, M. Auffray, Y. Tsuchiya, H. Nakanotani, C. Adachi, *Angew. Chem., Int. Ed.* **2021**, *60*, 19364.

[142] J. Lee, K. Shizu, H. Tanaka, H. Nakanotani, T. Yasuda, H. Kaji, C. Adachi, *J. Mater. Chem. C* **2015**, *3*, 2175.

[143] M. Okazaki, Y. Takeda, P. Data, P. Pander, H. Higginbotham, A. P. Monkman, S. Minakata, *Chem. Sci.* **2017**, *8*, 2677.

[144] D. Zhong, Y. Yu, L. Yue, X. Yang, L. Ma, G. Zhou, Z. Wu, *Chem. Eng. J.* **2021**, *413*, 127445.

[145] C.-H. Lim, M. D. Ryan, B. G. McCarthy, J. C. Theriot, S. M. Sartor, N. H. Damrauer, C. B. Musgrave, G. M. Miyake, *J. Am. Chem. Soc.* **2017**, *139*, 348.

[146] D. Koyama, H. J. Dale, A. J. Orr-Ewing, *J. Am. Chem. Soc.* **2018**, *140*, 1285.

[147] M. V. Bobo, J. J. Kuchta, A. K. Vannucci, *Org. Biomol. Chem.* **2021**, *19*, 4816.

[148] A. F. Buene, D. M. Almenningen, *J. Mater. Chem. C* **2021**, *9*, 11974.

[149] S. N. Al-Ghamdi, H. A. Al-Ghamdi, R. M. El-Shishtawy, A. M. Asiri, *Dyes Pigm.* **2021**, *194*, 109638.

[150] J. Shi, J. Chen, Z. Chai, H. Wang, R. Tang, K. Fan, M. Wu, H. Han, J. Qin, T. Peng, *J. Mater. Chem.* **2012**, *22*, 18830.

[151] S. Ergun, C. F. Elliott, A. P. Kaur, S. R. Parkin, S. A. Odom, *J. Phys. Chem. C* **2014**, *118*, 14824.

[152] D.-Y. Lee, H.-S. Lee, H.-S. Kim, H.-Y. Sun, D.-Y. Seung, *Korean J. Chem. Eng.* **2002**, *19*, 645.

[153] Z. Niu, H. Wu, L. Liu, G. Dai, S. Xiong, Y. Zhao, X. Zhang, *J. Mater. Chem. A* **2019**, *7*, 10581.

[154] G. Dai, Y. He, Z. Niu, P. He, C. Zhang, Y. Zhao, X. Zhang, H. Zhou, *Angew. Chem.* **2019**, *131*, 10007.

[155] B. M. Peterson, C. N. Gannett, L. Melecio-Zambrano, B. P. Fors, H. Abruña, *ACS Appl. Mater. Interfaces* **2021**, *13*, 7135.

[156] C. N. Gannett, B. M. Peterson, L. Melecio-Zambrano, C. Q. Trainor, B. P. Fors, H. D. Abruña, *J. Mater. Chem. A* **2021**, *9*, 5657.

[157] C. N. Gannett, B. M. Peterson, L. Shen, J. Seok, B. P. Fors, H. D. Abruña, *ChemSusChem* **2020**, *13*, 2428.

[158] W. Ma, L. W. Luo, P. Dong, P. Zheng, X. Huang, C. Zhang, J. X. Jiang, Y. Cao, *Adv. Funct. Mater.* **2021**, *31*, 2105027.

[159] M. J. Ohlow, B. Moosmann, *Drug Discov.* **2011**, *16*, 119.

[160] C. Iuga, A. Campero, A. Vivier-Bunge, *RSC Adv.* **2015**, *5*, 14678.

[161] S. Lee, K. Lee, K. Ku, J. Hong, S. Y. Park, J. E. Kwon, K. Kang, *Adv. Energy Mater* **2020**, *10*, 2001635.

[162] M. Kolek, F. Otteny, J. Becking, M. Winter, B. Esser, P. Bieker, *Chem. Mater.* **2018**, *30*, 6307.

[163] F. Otteny, M. Kolek, J. Becking, M. Winter, P. Bieker, B. Esser, *Adv. Energy Mater.* **2018**, *8*, 1802151.

[164] V. Perner, D. Diddens, F. Otteny, V. Küpers, P. Bieker, B. Esser, M. Winter, M. Kolek, *ACS Appl. Mater. Interfaces* **2021**, *13*, 12442.

[165] F. Otteny, G. Studer, M. Kolek, P. Bieker, M. Winter, B. Esser, *ChemSusChem* **2020**, *13*, 2232.

[166] F. Otteny, V. Perner, C. Einholz, G. Desmaizieres, E. Schleicher, M. Kolek, P. Bieker, M. Winter, B. Esser, *ACS Appl. Energy Mater.* **2021**, *4*, 7622.

[167] P. Acker, L. Rzesny, C. F. Marchiori, C. M. Araujo, B. Esser, *Adv. Funct. Mater.* **2019**, *29*, 1906436.

[168] B. M. Peterson, D. Ren, L. Shen, Y.-C. M. Wu, B. Ulgut, G. W. Coates, H. C. D. Abruña, B. P. Fors, *ACS Appl. Energy Mater.* **2018**, *1*, 3560.

[169] M. Rajesh, F. Dolhem, C. Davoisne, M. Becuwe, *ChemSusChem* **2020**, *13*, 2364.

[170] K. Lee, I. E. Serdiuk, G. Kwon, D. J. Min, K. Kang, S. Y. Park, J. E. Kwon, *Energy Environ. Sci.* **2020**, *13*, 4142.

[171] X. Zhang, Q. Xu, S. Wang, Y. Tang, X. Huang, *ACS Appl. Energy Mater.* **2021**, *4*, 11787.

[172] Z. Meng, Y. Zhang, M. Dong, Y. Zhang, F. Cui, T.-P. Loh, Y. Jin, W. Zhang, H. Yang, Y. Du, *J. Mater. Chem. A* **2021**, *9*, 10661.

[173] B. Häupler, R. Burges, T. Janoschka, T. Jähnert, A. Wild, U. S. Schubert, *J. Mater. Chem. A* **2014**, *2*, 8999.

[174] H. Nishide, K. Oyaizu, *Science* **2008**, *319*, 737.

[175] Y. Xie, K. Zhang, Y. Yamauchi, K. Oyaizu, Z. Jia, *Mater. Horiz.* **2021**, *8*, 803.

[176] J. Qu, T. Fujii, T. Katsumata, Y. Suzuki, M. Shiotsuki, F. Sanda, M. Satoh, J. Wada, T. Masuda, *J. Polym. Sci. A: Polym. Chem.* **2007**, *45*, 5431.

[177] J. Qu, T. Katsumata, M. Satoh, J. Wada, T. Masuda, *Macromolecules* **2007**, *40*, 3136.

[178] T. Suga, S. Sugita, H. Ohshiro, K. Oyaizu, H. Nishide, *Adv. Mater.* **2011**, *23*, 751.

[179] T. Sukegawa, A. Kai, K. Oyaizu, H. Nishide, *Macromolecules* **2013**, *46*, 1361.

[180] K. Zhang, Y. Hu, L. Wang, M. J. Monteiro, Z. Jia, *ACS Appl. Mater. Interfaces* **2017**, *9*, 34900.

[181] K. Zhang, Y. Hu, L. Wang, J. Fan, M. J. Monteiro, Z. Jia, *Polym. Chem.* **2017**, *8*, 1815.

[182] C. Friebe, U. S. Schubert, *Electrochemical Energy Storage: Next Generation Battery Concepts*, (Ed: R.-A. Eichel), Springer International Publishing, Cham **2019**, p. 65.

[183] K. Oyaizu, H. Nishide, *Adv. Mater.* **2009**, *21*, 2339.

[184] H. Nishide, T. Suga, *Electrochem. Soc. Interface.* **2005**, *14*, 32.

[185] L. Ji, J. Shi, J. Wei, T. Yu, W. Huang, *Adv. Mater.* **2020**, *32*, 1908015.

[186] D. R. Nevers, F. R. Brushett, D. R. Wheeler, *J. Power Sources* **2017**, *352*, 226.

[187] S. Wang, A. M. G. Park, P. Flouda, A. D. Easley, F. Li, T. Ma, G. D. Fuchs, J. L. Lutkenhaus, *ChemSusChem* **2020**, *13*, 2371.

[188] F. Li, S. Wang, Y. Zhang, J. L. Lutkenhaus, *Chem. Mater.* **2018**, *30*, 5169.

[189] L. Assumma, Y. Kervella, J. M. Mouesca, M. Mendez, V. Maurel, L. Dubois, T. Gutel, S. Sadki, *ChemSusChem* **2020**, *13*, 2419.

[190] C.-H. Lin, J.-T. Lee, D.-R. Yang, H.-W. Chen, S.-T. Wu, *RSC Adv.* **2015**, *5*, 33044.

[191] J.-K. Kim, *J. Power Sources* **2020**, *477*, 228670.

[192] W. Choi, S. Ohtani, K. Oyaizu, H. Nishide, K. E. Geckeler, *Adv. Mater.* **2011**, *23*, 4440.

[193] Y. Kim, C. Jo, J. Lee, C. W. Lee, S. Yoon, *J. Mater. Chem.* **2012**, *22*, 1453.

[194] B. Ernould, O. Bertrand, A. Minoia, R. Lazzaroni, A. Vlad, J.-F. Gohy, *RSC Adv.* **2017**, *7*, 17301.

[195] C. Lu, G. Pan, Q. Huang, H. Wu, W. Sun, Z. Wang, K. Sun, *J. Mater. Chem. A* **2019**, *7*, 4438.

[196] Y. Li, Z. Jian, M. Lang, C. Zhang, X. Huang, *ACS Appl. Mater. Interfaces* **2016**, *8*, 17352.

[197] T. Zhou, W. Jin, W. Xue, B. Dai, C. Feng, X. Huang, P. Théato, Y. Li, *J. Power Sources* **2021**, *483*, 229136.

[198] W. Jin, T. Zhou, Z. Wang, W. Xue, C. Feng, F. Zhang, X. Huang, D. Yang, P. Théato, Y. Li, *J. Power Sources* **2021**, *511*, 230363.

[199] H. Byeon, B. Gu, H.-J. Kim, J. H. Lee, I. Seo, J. Kim, J. W. Yang, J.-K. Kim, *Chem. Eng. J.* **2021**, *413*, 127402.

[200] T. Liu, X. Wei, Z. Nie, V. Sprenkle, W. Wang, *Adv. Energy Mater* **2016**, *6*, 1501449.

[201] C. DeBruler, B. Hu, J. Moss, X. Liu, J. Luo, Y. Sun, T. L. Liu, *Chem* **2017**, *3*, 961.

[202] A. Jouhara, E. Quarez, F. Dolhem, M. Armand, N. Dupre, P. Poizot, *Angew. Chem.* **2019**, *131*, 15827.

[203] M. Chen, L. Liu, P. Zhang, H. Chen, *RSC Adv.* **2021**, *11*, 24429.

[204] T. Ma, L. Liu, J. Wang, Y. Lu, J. Chen, *Angew. Chem., Int. Ed.* **2020**, *59*, 11533.

[205] P. Acker, M. E. Speer, J. S. Wössner, B. Esser, *J. Mater. Chem. A* **2020**, *8*, 11195.

[206] S. S. Hanson, E. Doni, K. T. Traboulsee, G. Coulthard, J. A. Murphy, C. A. Dyker, *Angew. Chem., Int. Ed.* **2015**, *54*, 11236.

[207] F. Alkhayri, C. A. Dyker, *J. Electrochem. Soc.* **2020**, *167*, 160548.

[208] Z. Burešová, M. Klikar, P. Mazúr, M. Mikešová, J. Kvíčala, T. Bystron, F. Bureš, *Front. Chem.* **2021**, *8*, 631477.

[209] J. S. Bus, S. D. Aust, J. E. Gibson, *Biochem. Biophys. Res. Commun.* **1974**, *58*, 749.

[210] M. Cave, K. C. Falkner, C. McClain, in *Zakim And Boyer's Hepatology (Sixth Edition)*, (Eds: T. D. Boyer, M. P. Manns, A. J. Sanyal), W.B. Saunders, Saint Louis **2012**, p. 476.

[211] I. A. Rodríguez-Pérez, Z. Jian, P. K. Waldenmaier, J. W. Palmisano, R. S. Chandrabose, X. Wang, M. M. Lerner, R. G. Carter, X. Ji, *ACS Energy Lett.* **2016**, *1*, 719.

[212] S. Dong, Z. Li, I. A. Rodríguez-Pérez, H. Jiang, J. Lu, X. Zhang, X. Ji, *Nano Energy* **2017**, *40*, 233.

[213] M. Kato, T. Masese, M. Yao, N. Takeichi, T. Kiyobayashi, *New J. Chem.* **2019**, *43*, 1626.

[214] D. Ogi, Y. Fujita, M. Kato, T. Yamauchi, T. Shirahata, M. Yao, Y. Misaki, *Eur. J. Org. Chem.* **2019**, *2019*, 2725.

[215] B. Häupler, R. Burges, C. Friebe, T. Janoschka, D. Schmidt, A. Wild, U. S. Schubert, *Macromol. Rapid Commun.* **2014**, *35*, 1367.

[216] Y. Inatomi, N. Hojo, T. Yamamoto, S.-I. Watanabe, Y. Misaki, *ChemPlusChem* **2012**, *77*, 973.

[217] M. Kato, K.-I. Senoo, M. Yao, Y. Misaki, *J. Mater. Chem. A* **2014**, *2*, 6747.

[218] Y. Zu, Y. Xu, L. Ma, Q. Kang, J. Wang, H. Yao, J. Hou, Y. Zu, Y. Xu, L. Ma, Q. Kang, J. Wang, H. Yao, J. Hou, *Energy Storage Mater.* **2021**, *41*, 240.

[219] Y. Fujihara, H. Kobayashi, S. Takaishi, T. Tomai, M. Yamashita, I. Honma, *ACS Appl. Mater. Interfaces* **2020**, *12*, 25748.

[220] L. Wu, F. Wu, Q. Sun, J. Shi, A. Xie, X. Zhu, W. Dong, *J. Mater. Chem. C* **2021**, *9*, 3316.

[221] J. Cho, Y. J. Kim, B. Park, *Chem. Mater.* **2000**, *12*, 3788.

[222] X. Huang, Y. Yao, F. Liang, Y. Dai, *J. Alloys Compd.* **2018**, *743*, 763.

[223] Y. Cai, Y. Huang, X. Wang, D. Jia, W. Pang, Z. Guo, Y. Du, X. Tang, *J. Power Sources* **2015**, *278*, 574.

[224] C. Su, H. He, L. Xu, K. Zhao, C. Zheng, C. Zhang, *J. Mater. Chem. A* **2017**, *5*, 2701.

[225] F. A. Obrezkov, A. F. Shestakov, V. F. Traven, K. J. Stevenson, P. A. Troshin, *J. Mater. Chem. A* **2019**, *7*, 11430.

[226] X. Wang, G. Li, Y. Han, F. Wang, J. Chu, T. Cai, B. Wang, Z. Song, *ChemSusChem* **2021**, *14*, 3174.

[227] J. Lv, J. Ye, G. Dai, Z. Niu, Y. Sun, X. Zhang, Y. Zhao, *J. Energy Chem.* **2020**, *47*, 256.

[228] Y. Zhang, P. Gao, X. Guo, H. Chen, R. Zhang, Y. Du, B. Wang, H. Yang, *RSC Adv.* **2020**, *10*, 16732.

[229] K. Hatakeyama-Sato, S. Matsumoto, H. Takami, T. Nagatsuka, K. Oyaizu, *Macromol. Rapid Commun.* **2021**, *42*, 2100374.

[230] S. Yeşilot, F. Hacıvelioğlu, S. Küçükköylü, K. B. Çelik, G. Sayan, R. Demir-Cakan, *Macromol. Chem. Phys.* **2017**, *218*, 1700051.

[231] S. Wang, Q. Wang, P. Shao, Y. Han, X. Gao, L. Ma, S. Yuan, X. Ma, J. Zhou, X. Feng, B. Wang, *J. Am. Chem. Soc.* **2017**, *139*, 4258.

[232] Y. Liu, Z. Niu, G. Dai, Y. Chen, H. Li, L. Huang, X. Zhang, Y. Xu, Y. Zhao, *Mater. Today Energy* **2021**, *21*, 100812.

[233] A. A. Golriz, T. Suga, H. Nishide, R. Berger, J. S. Gutmann, *RSC Adv.* **2015**, *5*, 22947.

[234] T. Sarukawa, N. Oyama, *J. Electrochem. Soc.* **2010**, *157*, F23.

[235] K. Sakaushi, E. Hosono, G. Nickerl, H. Zhou, S. Kaskel, J. Eckert, *J. Power Sources* **2014**, *245*, 553.

[236] Z. Zhang, L. Hu, H. Wu, W. Weng, M. Koh, P. C. Redfern, L. A. Curtiss, K. Amine, *Energy Environ. Sci.* **2013**, *6*, 1806.

[237] X. Fan, C. Wang, *Chem. Soc. Rev.* **2021**, *50*, 10486.

[238] W. Zhou, M. Zhang, X. Kong, W. Huang, Q. Zhang, *Adv. Sci.* **2021**, *8*, 2004490.

[239] L. Zhao, A. E. Lakraychi, Z. Chen, Y. Liang, Y. Yao, *ACS Energy Lett.* **2021**, *6*, 3287.

**ADVANCED
SCIENCE NEWS**

www.advancedsciencenews.com

**ADVANCED
ENERGY & SUSTAINABILITY
RESEARCH**
Open Access

www.advenergysustres.com

[240] X. Zhang, W. Zhou, M. Zhang, Z. Yang, W. Huang, *J. Energy Chem.* **2021**, *52*, 28.

[241] X. Wang, Z. Shang, A. Yang, Q. Zhang, F. Cheng, D. Jia, J. Chen, *Chem* **2019**, *5*, 364.

[242] J. Bitenc, A. Vizintin, J. Grdadolnik, R. Dominko, *Energy Storage Mater.* **2019**, *21*, 347.

[243] L. Sieuw, A. Jouhara, É. Quarez, C. Auger, J.-F. Gohy, P. Poizot, A. Vlad, *Chem. Sci.* **2019**, *10*, 418.

Hyojin Kye received her B.Sc. degree (2019) in chemical engineering at Konkuk University and is a graduate student as a Ph.D. candidate in organic and nano system engineering at Konkuk University under the advisory of Prof. Bong-Gi Kim. Her research interests are organic cathode materials for lithium-ion batteries.

Ji Eon Kwon is currently a senior researcher at the Korea Institute of Science and Technology (KIST). He received his B.S. and Ph.D. degrees from Seoul National University. His achievements are honored by prestigious fellowships such as Brain Korea 21 Plus and Korea Presidential Post-Doc Fellowship. His research focuses on developing novel organic and polymeric electrode materials for various types of batteries.

Bong-Gi Kim is the department chair of organic and nano system engineering at Konkuk University in the Republic of Korea and an associate faculty in the division of chemical engineering. He received his Ph.D. degree in macromolecular science and engineering from University of Michigan (Ann Arbor) in 2012. His primary research interests are designing semiconducting materials for optical, electrical, and electrochemical applications. His research team has established effective material design strategies for self-alignment, self-assembly, and molecular doping of organic semiconductor. Currently, he is focusing on the development of organic redox active materials for organic batteries.